



# Application of a novel [3+2] cycloaddition reaction to prepare substituted imidazoles and their use in the design of potent DFG-out allosteric B-Raf inhibitors

Justin Dietrich<sup>a</sup>, Vijay Gokhale<sup>a</sup>, Xiadong Wang<sup>a</sup>, Laurence H. Hurley<sup>a,b,c</sup>, Gary A. Flynn<sup>a,c,\*,†</sup>

<sup>a</sup> Department of Pharmacology and Toxicology, College of Pharmacy, The University of Arizona, Tucson, AZ 85721, United States

<sup>b</sup> Arizona Cancer Center, University of Arizona, 1515 N. Campbell Avenue, Tucson, AZ 85724, United States

<sup>c</sup> BIOS Institute, University of Arizona, 1657 E. Helen Street, Tucson, AZ 85721, United States

## ARTICLE INFO

### Article history:

Received 12 September 2009

Revised 26 October 2009

Accepted 28 October 2009

Available online 11 November 2009

### Keywords:

B-Raf

p38

Type-II

Allosteric

Kinase inhibitor

Structure-base design

de novo

## ABSTRACT

B-Raf protein kinase, which is a key signaling molecule in the RAS–RAF–MEK–ERK signaling pathway, plays an important role in many cancers. The B-Raf V600E mutation represents the most frequent oncogenic kinase mutation known and is responsible for increased kinase activity in approximately 7% of all human cancers, establishing B-Raf as an important therapeutic target for inhibition. Through the use of an iterative program that utilized a chemocentric approach and a rational structure based design, we have developed novel, potent, and specific DFG-out allosteric inhibitors of B-Raf kinase. Here, we present efficient and versatile chemistry that utilizes a key one pot, [3+2] cycloaddition reaction to obtain highly substituted imidazoles and their application in the design of allosteric B-Raf inhibitors. Inhibitors based on this scaffold display subnanomolar potency and a favorable kinase profile.

© 2009 Elsevier Ltd. All rights reserved.

## 1. Introduction

B-Raf kinase, a Ser/Thr kinase, is mutated in approximately 7% of all human cancers with higher occurrence in 66% of human melanomas, 45% of sporadic papillary thyroid cancers, 33% of KRAS mutated pancreatic cancers, and 15% of sporadic colorectal cancers.<sup>1–6</sup> The most common B-Raf oncogenic mutation is a single-base missense substitution (T to A at nucleotide 1799) that is found in 90% of all B-Raf mutated cancers and involves a valine to glutamic acid substitution at codon 600 (V600E).<sup>7</sup> This mutation is found adjacent to serine 599, which is phosphorylated during activation of the kinase.<sup>8</sup> The polarity of glutamic acid in the V600E mutation mimics the polarity of serine phosphorylation in the kinase activation loop, resulting in constitutive activation of the MAPK pathway and a 500-fold increase in B-Raf activity exclusive of extracellular growth factor signaling.<sup>9,10</sup>

The most studied B-Raf inhibitor, Sorafenib (Bay 43-9006, Nexavar<sup>®</sup>), was approved by the FDA in 2005 for the treatment

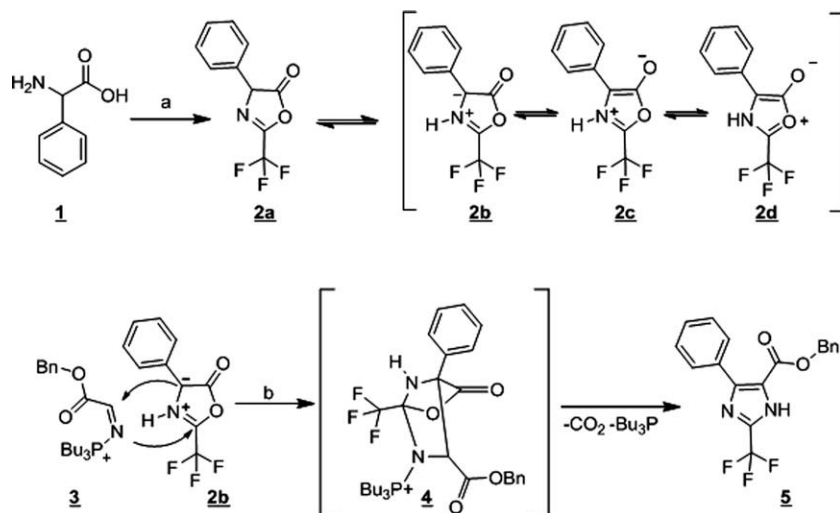
of renal cell carcinoma and in 2007 for the treatment of hepatocellular carcinoma, and is still undergoing multiple clinical trials in other types of cancer.<sup>3,11,12</sup> This agent, even though it was designed as a B-Raf inhibitor, has failed to demonstrate significant improvement in the prognosis of cancers that harbor the V600E mutation when compared to cancers without this prevalent oncogenic mutation.<sup>13</sup> The failure can be attributed to the lack of selectivity of Sorafenib which also inhibits many other kinases, such as VEGFR1–3, PDGFR-B, c-ABI, FLT-3, c-Kit, and p38 $\alpha$ .<sup>14,15</sup> In renal cell carcinoma, the promising clinical efficacy of Sorafenib is attributed to the combination of inhibiting VEGFR-2, PDGFRB, and B-Raf, a serendipitous mix for highly vascularized renal cell carcinomas, which often overexpress the pro-angiogenic receptor tyrosine kinases VEGF-R and PDGFR-B.<sup>16,17</sup> In the treatment of B-Raf mutant cancers, however, the lack of selectivity may be the Achilles' heel that limits the efficacy by creating dose-limiting off-target toxicity. The development of more potent and specific inhibitors of the B-Raf V600E mutant enzyme can provide insight into the true therapeutic potential of targeting B-Raf in cancers that harbor a B-Raf mutation.

We have utilized a chemocentric approach in which we first invested in the development of a robust chemistry that yielded molecules with three sites of variation and then applied this chemistry as a scaffold for the production of highly potent B-Raf inhibitors.

\* Corresponding author. Tel.: +1 520 250 9208; fax: +1 520 575 6050.

E-mail addresses: [dietrich@pharmacy.arizona.edu](mailto:dietrich@pharmacy.arizona.edu) (J. Dietrich), [hurley@pharmacy.arizona.edu](mailto:hurley@pharmacy.arizona.edu) (L.H. Hurley), [flynn@pharmacy.arizona.edu](mailto:flynn@pharmacy.arizona.edu), [flynn@tuc@aol.com](mailto:flynn@tuc@aol.com) (G.A. Flynn).

† Present address: Spacefill Enterprises LLC, 9750N. Cliff View Place, Tucson, AZ 85704, United States.



**Scheme 1.** [3+2] Route to tri-substituted imidazoles. Reagents and conditions: (a) 2 equiv, TFAA, 2 h; (b) 1.0 equiv,  $\text{PBu}_3$ , 1.1 equiv, benzyl cyanofornate, toluene, 8 h.

## 2. Chemistry approach

The chemocentric approach to kinase inhibitors taken here is based on a relatively obscure yet highly efficient entrance to tri-substituted imidazoles that was first described in a Japanese patent (WO9504724)<sup>18</sup> in 1995 for the production of pesticides. Although the detailed mechanism for this reaction is not well described, it likely involves a [3+2] cycloaddition reaction as the key step (Scheme 1). The flexible synthesis begins with reaction of phenylglycine **1** with 2–3 equiv of trifluoroacetic anhydride under neat conditions. The trifluoromethylacetamide that initially forms undergoes further in situ cyclo-dehydration resulting in formation of  $\Delta^2$ -oxazolinone **2a** in near quantitative yield.

It is well accepted that  $\Delta^2$ -oxazolinones exist as tautomers of the three mesoionic oxazolium 5-oxides: **2b**, **2c**, and **2d**.<sup>19</sup> The resonance form **2b** represents a cyclic, aromatic azomethine ylide that has been utilized previously as a 1,3-dipole in other cycloaddition reactions.<sup>20–22</sup> For example, in the presence of a dipolarophile, such as dimethyl acylenedicarboxylate, 2,4-disubstituted  $\Delta^2$ -oxazolinones can undergo a facile 1,3-dipolar [3+2] cycloaddition reaction to form pyrroles.<sup>19</sup> In the approach to imidazoles described here, it is assumed that benzyl 2-(tributylphosphoniumimino)-acetate **3** is the actual dipolarophile, which was generated in situ from benzylcyanofornate and tributylphosphine. Initial adduct **4**, produced by reaction of this dipolarophile with azomethine ylide **2b** in a [3+2] manner, rapidly collapses with evolution of  $\text{CO}_2$  and aromatization to yield the 2,4,5-tri-substituted imidazole. Overall yields for this one-pot procedure are typically 60–70%.

## 3. Inhibitor design and molecular modeling

Inhibitor design was guided by a pharmacophore model derived from recent crystal structures of three known DFG-out allosteric kinase inhibitors: Imatinib (Gleevec<sup>®</sup>, STI571, pdb 2HYY), Sorafenib (Nexavar<sup>®</sup>, BAY 43-9006, pdb 1UWH), and BIRB-796 (pdb 1KV2), which collectively illustrate common interactions necessary for high-affinity binding to the DFG-out allosteric pocket of these kinases. The allosteric binding site is an inactive conformation of the enzyme characterized by the movement of an Asp-Phe-Gly (DFG) loop. The binding site is made accessible by a rearrangement of the activation loop and subsequent movement of a phenylalanine side chain out of a large hydrophobic pocket and into the ATP binding site. This movement results in a conformation that is mutually exclusive to ATP binding and also creates

a large hydrophobic pocket that allosteric kinase inhibitors bind to, stabilizing and thus increasing the population of an inactive conformation of the enzyme. Inhibitors that bind this site often exhibit slow binding kinetics.

The three DFG-out type-II allosteric kinase inhibitors described above share a basic architecture that can be defined by four key interactions (Sorafenib is used as an example in Fig. 1). A critical inhibitor interacting group is the central core or scaffold, which establishes a bridging hydrogen-bond network between a conserved glutamate side chain and the amide N–H from the aspartate involved in the movement of the DFG loop. Sorafenib utilizes a phenyl urea to perform this function. The second interaction is at the selectivity site, which is created when the phenyl alanine of the DFG loop vacates its lipophilic pocket. Sorafenib contains a *meta*-trifluoromethyl-*para*-chlorophenyl ring that occupies this hydrophobic pocket. The third interaction site is in the ‘gatekeeper region,’ which is close to a conserved lysine side chain that is normally involved in triphosphate binding. As a result of the DFG loop movement, the phenylalanine side chain of this loop typically closes off the gatekeeper region, forming a distinct binding site that is attractive for edge on aromatic–aromatic interactions. The fourth interaction site is known as the ‘hinge region,’ which normally binds the flat aromatic adenine ring of ATP and establishes crucial hydrogen bonds with both ‘ATP site’ and ‘allosteric site’ inhibitors.

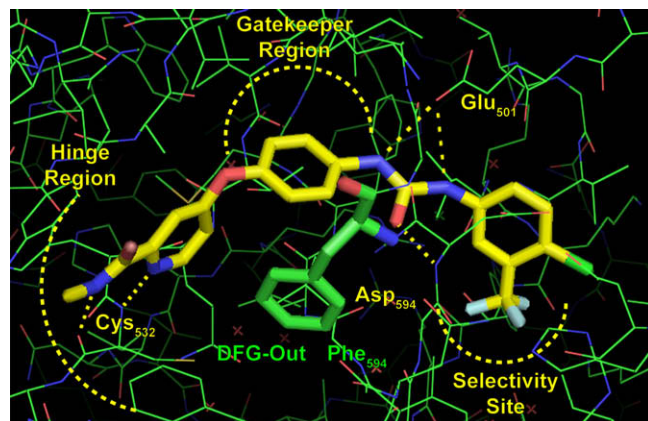


**Figure 1.** Crystal structure of Sorafenib (Nexavar<sup>®</sup>, BAY 43-9006) bound to B-Raf kinase.

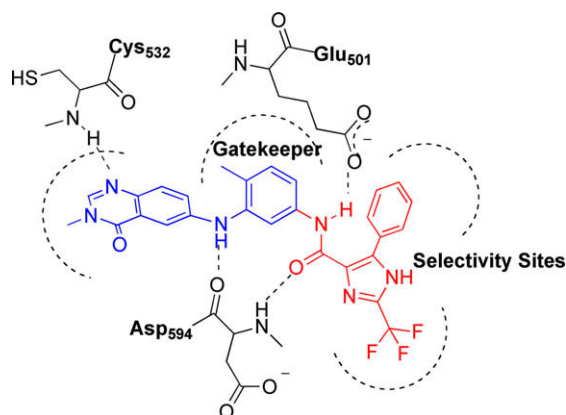


**Figure 2.** Two-dimensional structure of the rational design of imidazole-based inhibitors.

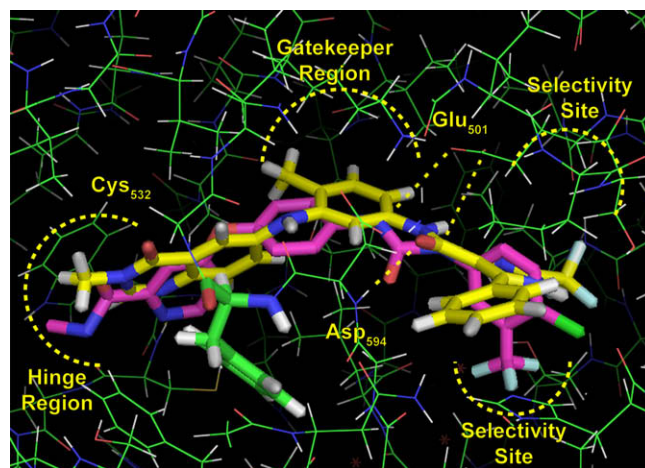
The *N*-methyl picolinamide moiety of Sorafenib contributes these interactions.

We applied the imidazole chemistry described above in the design of novel allosteric DFG-out B-Raf inhibitors by incorporating a tri-substituted imidazole as the central core scaffold (Fig. 2, red). The carboxamide function at the 4-position of the imidazole ring was expected to make critical hydrogen bonding interactions with Glu501 and Asp594 while the substituents at the 2- and 5-positions of the imidazole ring could be easily varied to optimize the hydrophobic interactions within the selectivity site. A known hinge region binding motif, 6-[(5-amino-2-methylphenyl)amino-3-methyl-quinazolin-4(3*H*)-one (QUIN), that was previously reported to bind the hinge region with good affinity, was used to anchor the hinge region (Fig. 2, blue).<sup>23</sup> We chose to incorporate a trifluoromethyl group at the 2-position of the imidazole ring because the trifluoromethyl group had been used successfully in Sorafenib and because the electron withdrawing effects of the trifluoromethyl group could potentially limit the ability of the imidazole nitrogen to non-specifically chelate metals and inhibit cytochrome P450s.

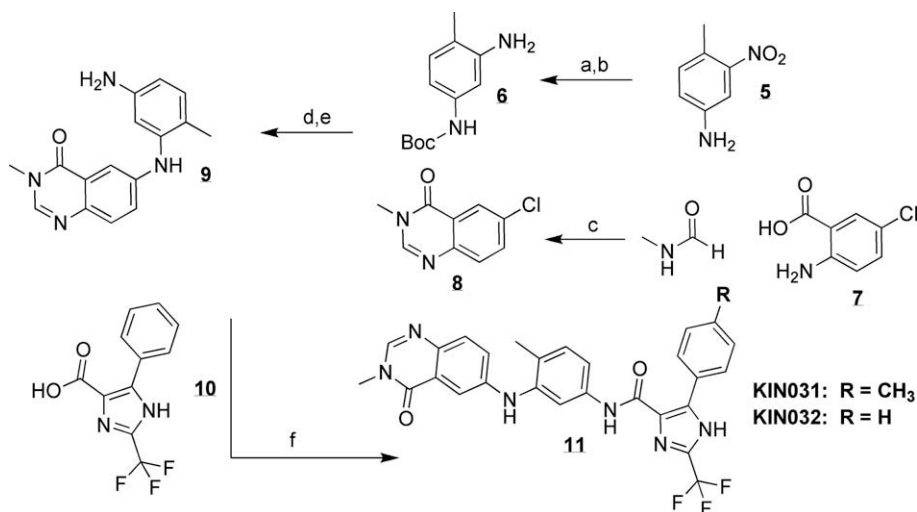
Assembly of the QUIN fragment and the final imidazole-quinazolinone containing inhibitors is shown in Scheme 2. The QUIN fragment **9**, was obtained through a neat reaction of 5-chloroanthranilic acid **7** with methyl formamide at 160 °C for 8 h followed by

a Buchwald aromatic amination of the resulting 6-chloroquinazolinone **8** with *tert*-butyl 3-amino-4-methylphenylcarbamate **6**. Subsequent deprotection in 10% trifluoroacetic acid in dichloromethane produced amine **9**, which was then coupled to 5-phenyl-2-(trifluoromethyl)-1*H*-imidazole-4-carboxylic acid **10** under standard EDC coupling conditions.

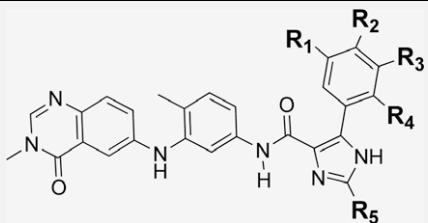
Putative designs were docked with the unliganded structure of B-Raf kinase (crystal structure coordinates with Sorafenib, pdb 1UWH) and p38 $\alpha$  (crystal structure coordinates with BIRB 796, pdb 1KV2) using a FLEX–FLEXIDOCK protocol (as described in Computational Methods). Each molecule was initially docked using the FLEX program, and the best docking pose was then refined with FLEXIDOCK (both flexible ligand and flexible protein side chains). Docking orientations from FLEXIDOCK were analyzed using two criteria: docking score and number of interactions in the binding pocket. The crystal structure of Sorafenib bound to B-Raf was used as a reference for comparison. Two molecules which differed by the inclusion of a *para*-methyl substituent (R = H or R = Me, Scheme 2) were used to test our initial hypothesis. When evaluating the



**Figure 3.** Docked imidazole-quinazolinone binding structure. Docked model of KIN032 (yellow) in the crystal structure 1UWH overlapped with Sorafenib (mauve). The trifluoromethyl phenyl ring of Sorafenib sits comfortably in the selectivity site. The imidazole scaffold is unable to utilize this space and twists orthogonal to the selectivity sites.



**Scheme 2.** Route to imidazole quinazolinones. Reagents and conditions: (a) Boc<sub>2</sub>O, THF, 65 °C, overnight, 83% yield; (b) 40 psi H<sub>2</sub>, 10% Pd/C, EtOH, 15 h, 92% yield; (c) 160 °C, 8 h, 65% yield; (d) 1.4 equiv, *t*-BuONa, 3% Pd<sub>2</sub>(dba)<sub>3</sub>, 5% dbbp, 8 h, 82% yield; (e) 10% TFA/DCM, 1 h, 94% yield; (f) **5**, 1.1 equiv, EDCI, 1.3 equiv, HOAt, 4 equiv, DIPEA, DCM, 54.7% yield.

**Table 1**Biochemical data generated for the QUIN series of imidazoles (results were calculated from the average of  $n \geq 2$  independent experiments performed in duplicate with  $R^2 > 0.93$ )


	R1	R2	R3	R4	R5	IC <sub>50</sub> B-Raf V600E (nM)	IC <sub>50</sub> P38 $\alpha$ (nM)	S.I.
Sorafenib	H	H	H	H	CF <sub>3</sub>	120.1	84.2	0.7
KIN032	H	H	H	H	CF <sub>3</sub>	21.4	405.2	18.9
KIN031	H	CH <sub>3</sub>	H	H	CF <sub>3</sub>	27.9	1648.0	59.1
KIN035	H	F	H	H	CF <sub>3</sub>	0.4	16.0	38.8
KIN036	Cl	F	H	H	CF <sub>3</sub>	53.2	48.8	0.9
KIN037	CH <sub>3</sub>	F	H	H	CF <sub>3</sub>	19.7	60.1	3.0
KIN038	F	CH <sub>3</sub>	H	H	CF <sub>3</sub>	0.3	100.2	312.1
KIN039	OCH <sub>3</sub>	OCH <sub>3</sub>	OCH <sub>3</sub>	H	CF <sub>3</sub>	292.4	94.4	0.3
KIN040	CF <sub>3</sub>	H	H	H	CF <sub>3</sub>	49.6	105.2	2.1
KIN041	H	H	H	CF <sub>3</sub>	CF <sub>3</sub>	112.3	468.4	4.2
KIN057	F	F	H	H	CF <sub>3</sub>	0.3	11.0	35.8
KIN042	H	CH <sub>3</sub>	H	H	<i>t</i> -But	91.3	96.3	1.1
KIN043	H	H	H	H	Phe	48.3	121.7	2.5

docked model of KIN032 bound to the empty B-Raf crystal structure 1UWH, the conformation of these inhibitor designs did not match the binding conformation expected and the docked conformation appeared to be energetically unfavorable (Fig. 3). Although the QUIN moiety interacted as expected to the hinge and gate-keeper regions, the imidazole core scaffold at the DFG-out selectivity site was required to twist within the selectivity site to relieve sterical clashes with the protein. This twisting diminished the lipophilic interactions within the selectivity sites and our calculations also suggested that the imidazole carboxamide function was unlikely to easily make the important hydrogen bonding interactions with Glu501 and Asp594 that are required for a potent inhibitor. In spite of the negative indications for B-Raf binding, these two putative inhibitors (KIN031, R = 4-Me and KIN032 R = H) were prepared and tested against both B-Raf and p38 $\alpha$ . The positive results obtained (Table 1) pointed to some new information about the B-Raf 'allosteric' binding site.

#### 4. Biochemical assays and initial feedback

KIN031, KIN032, and Sorafenib were tested in two in vitro <sup>32</sup>P SDS-PAGE gel kinase assays, one for B-Raf V600E and one for p38 $\alpha$ , an alternate model kinase that is known to exist in the DFG-out conformation. Sorafenib potently inhibits p38 $\alpha$  with a reported IC<sub>50</sub> of 38 nM<sup>15</sup> and BIRB-796, a potent p38 $\alpha$  inhibitor,<sup>24</sup> is similar in architecture to Sorafenib. Monumental efforts have been made by both major pharmaceutical and biotech companies to develop selective inhibitors of p38 $\alpha$  due to the major role this kinase plays in mediating inflammatory responses,<sup>25</sup> however, previous efforts to advance p38 $\alpha$  inhibitors in the clinic have been thwarted by toxicity issues, limited long term therapeutic benefit, and transient reductions in C-reactive protein (CRP) levels.<sup>26</sup> We were not interested in developing a p38 $\alpha$  inhibitor and moreover felt it might be desirable to tune out p38 $\alpha$  inhibition. We were interested in following the change in selectivity among these similar kinases as a probe to detect an overall change in the kinase selectivity of our molecules.

These assays utilized a high ATP concentration (200  $\mu$ M) which is greater than 10 times the Km of ATP for B-Raf V600E and p38 $\alpha$ <sup>27</sup> and full-length protein substrates, MEK1 for B-Raf V600E and MAPKAP-K2 for p38 $\alpha$ . As expected, these inhibitors exhibited slow binding kinetics, requiring a long pre-incubation (1 h) to allow

the equilibrium of the DFG loop to shift to the inactive state in which allosteric inhibitors bind.<sup>24</sup> Kinase assay results for KIN031 and KIN032 (Table 1) with respect to the V600E B-Raf mutant enzyme showed an IC<sub>50</sub> of 28 nM and 21 nM, respectively. Against p38 $\alpha$ , the IC<sub>50</sub>'s were 1648 nM and 405 nM, respectively. KIN031 had a selectivity index (IC<sub>50</sub>B-Raf/IC<sub>50</sub> p38) of 59.0 (Table 1) and KIN032 had a selectivity index of 18.9. In our assay, Sorafenib displayed an IC<sub>50</sub> of 120.3 nM for B-Raf V600E and an IC<sub>50</sub> of 84.2 nM for p38 $\alpha$ , resulting in a selectivity index of 0.70. When KIN031 is compared to Sorafenib, KIN031 is fourfold more potent against the V600E B-Raf mutant enzyme and 84-fold more selective over p38 $\alpha$ . These results were encouraging, as molecules that incorporated the designed imidazole carboxamide displayed increased potency and demonstrated that specific interactions made at the selectivity site could be modulated to tune selectivity and potency. The nanomolar potency displayed by KIN031 and KIN032, however, was not consistent with the predicted unfavorable binding mode generated by molecular modeling studies with the empty crystal structure of B-Raf (1UWH). This led us to search for alternate conformations or different binding modes, particularly in the selectivity site.

Plexxikon has recently reported a novel series of B-Raf inhibitors based on a 7-azaindole scaffold that inhibits B-Raf V600E with an IC<sub>50</sub> of 13 nM.<sup>28</sup> In the discovery of this molecule, Plexxikon was able to uncover new possible binding modes, which have provided a greater understanding of the extent of dynamic movement in the DFG-out type-II binding pocket of B-Raf. The crystal structure of the 7-aza indole inhibitor PLX4720 bound to B-Raf (pdb 3c4c) consists of two non-symmetrical monomers. One monomer depicts PLX4720 binding to the DFG-in conformation (Fig. 4a, green), which is the active conformation of the enzyme that ATP can bind to. The other monomer shows PLX4720 binding to the inactive conformation in which the phenylalanine of the DFG motif is moved and reveals the selectivity site (Fig. 4a, yellow). Atypical to most bound structures of B-Raf inhibitors, PLX4720 is able to induce movement of glutamate 501 deep into the selectivity site, approximately 10 Å away from its normal position. Consequentially, a unique salt bridge is formed between the side chains of Asp594 and Lysine483 (Fig. 4b) that stabilizes the DFG-out conformation of B-Raf.

When KIN032 was docked into the inhibitor free DFG-out monomer (pdb 3C4C), we found high complementation between

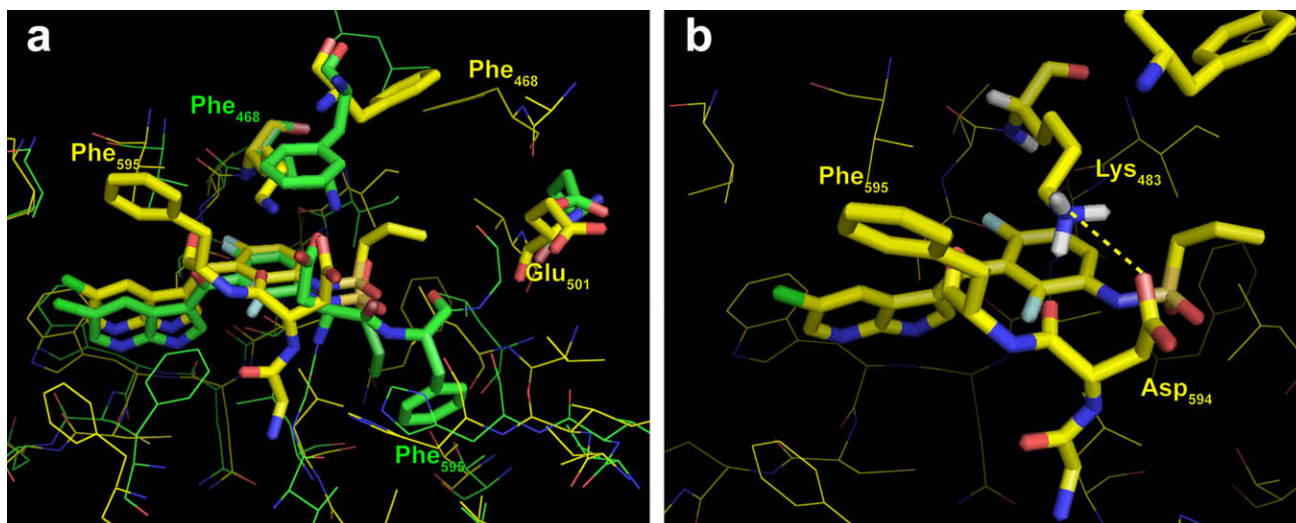


**Figure 4.** Structure of PLX4720 bound to B-Raf. (a) Overlay of the DFG-out (yellow) and DFG-in (green) monomers of B-Raf with PLX4720 bound (pdb 1C4C). Phe595 in the monomer depicted in yellow is in the DFG-out state. Glu501 sits far to the right in the allosteric binding site. (b) A unique salt bridge is shown between Asp594 and Lys483 in the DFG-out conformation.

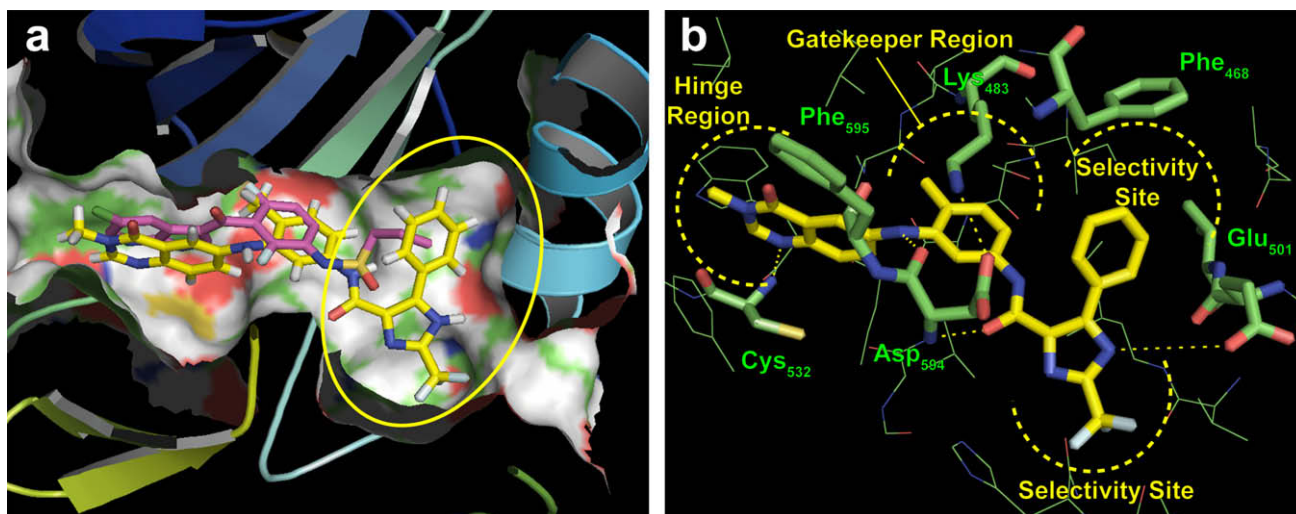


**Figure 5.** KIN032 bound to the Plexxikon structure. (a) Overlap of docked KIN032 (yellow) and crystal structure of PLX4720 (mauve) in pdb 3C4C. KIN032 utilizes more of the hydrophobic allosteric binding region (yellow oval). (b) Docked model of KIN032.

the small molecule and the protein (Fig. 5a). When this pose of KIN032 was overlapped and viewed together with the crystal structure of PLX4720 (Fig. 5a), both the hinge region quinazolinone ring system and the gatekeeper aryl group from KIN032 overlapped well with the 7-azaindole and gatekeeper ring systems of PLX4720. In this conformation, the quinazolinone ring system was able to easily accept a hydrogen bond from Cys532 in the hinge region. A unique property of PLX4720 allows placement of its diminutive *n*-propyl sulfonamide moiety shallowly into the selectivity site, leaving this pocket mostly empty (Fig. 5a). When docked into this alternative binding mode, KIN032 was able to occupy significantly more of the rearranged selectivity site. This is allowed because the side chain displacement of Glu501 creates a large hydrophobic pocket in the upper of the two selectivity sites. This new site is capped by the side chain of Phe468 and appears to be large enough to comfortably accommodate the imidazole-5-phenyl substituent while the 2-trifluoromethyl substituent occupies the lower selectivity site. Furthermore, in the tautomeric form shown in Figure 5b, the imidazole NH is capable of interacting with the carboxyl of the displaced Glu501 while the carbonyl portion of

the carboxamide linkage can easily establish a crucial hydrogen-bond with the backbone NH of Asp594.

The binding pocket depicted by the DFG-out monomer of PLX4720 bound to B-Raf V600E (pdb 3C4C) showed higher complementarity with KIN032 than the binding pocket utilized by Sorafenib (pdb 1UWH). To generate relevant SAR and validate the alternate binding mode in the selectivity site, ten additional compounds were synthesized (Table 1). The QUIN hinge region binding moiety (Fig. 6, red) was incorporated into all the molecules, and variations were made through substitution on the phenyl ring located at the 5-position of the imidazole ring (KIN031–KIN041, KIN057) or by making direct substitution at the 2-position of the imidazole ring (KIN042, KIN043) (Fig. 6, blue). Substitutions on the phenyl ring allowed us to explore specific interactions that are proposed for the putative upper selectivity site that was created when Glu501 was displaced from its normal position. Similarly, substitutions at the 2-position allowed us to theoretically explore the requirements of the lower selectivity site that was voided when phenylalanine switched conformation in the DFG loop move.

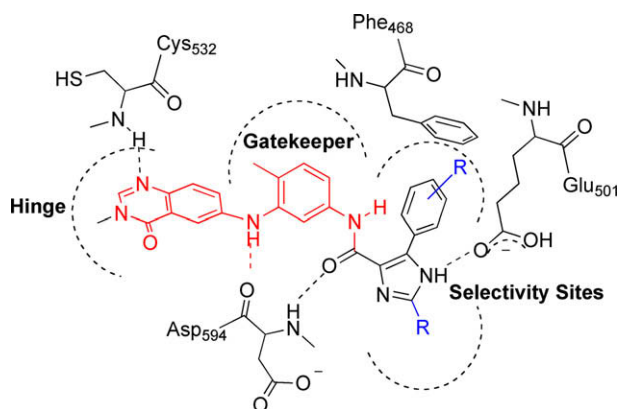


**Figure 6.** Schematic model of SAR design for imidazole-quinazolinone.

Biochemical feedback from the imidazole-quinazolinone series of compounds identified novel structure–activity relationships when the phenyl ring at the 5-position of the imidazole scaffold was substituted with various groups (Table 1). The kinase inhibition results determined for KIN035 illustrate how placement of a fluorine atom at the 4-position of the phenyl substituent on the imidazole ring leads to a distinct increase in potency for both B-Raf V600E and p38 $\alpha$  ( $IC_{50}$ 's = 0.4 nM and 16.0 nM) (Table 1). While fluorine was also well tolerated at the *meta* position (KIN038 and KIN057), any larger substituent such as  $-CH_3$  (KIN037),  $-OMe$

(KIN039), and  $-CF_3$  (KIN040), is not well tolerated resulting in decreased potency for both B-Raf V600E and p38 $\alpha$ . KIN038, incorporating a fluorine at the *meta* position and a methyl at the *para* position of the phenyl ring, retained subnanomolar potency for B-Raf V600E ( $IC_{50}$  = 0.3 nM), but disfavored p38 $\alpha$  inhibition ( $IC_{50}$  = 100.2 nM). This SAR mirrors that observed for KIN031 ( $IC_{50}$  B-Raf = 27.9,  $IC_{50}$  p38 = 1648 nM) compared to KIN032 ( $IC_{50}$  B-Raf = 21.4,  $IC_{50}$  p38 = 405.2 nM) where a *para*-methyl phenyl substituent was more tolerated by B-Raf than for p38 $\alpha$ .

Molecules that were modified at the 2-position of the imidazole scaffold (KIN042 and KIN043, Table 1) were used to evaluate the size of the hydrophobic pocket that was voided during the DFG loop move. Significantly, KIN042, in which the larger *t*-butyl group was substituted for trifluoromethyl (KIN031) at the 2-position of the imidazole ring, exhibited increased potency for p38 $\alpha$  ( $IC_{50}$  p38 = 96.3 nM,  $IC_{50}$  B-Raf = 91.3 nM) and decreased potency for B-Raf V600E when compared directly to KIN031 ( $IC_{50}$  B-Raf = 27.9,  $IC_{50}$  p38 = 1648 nM) (Table 1). As a result, KIN042 displayed a selectivity index ( $SI = IC_{50}$  B-Raf/ $IC_{50}$  p38) of 1.1 compared to KIN031, which displayed a selectivity index of 59.1.

Similarly, comparison of KIN043 ( $SI = 2.5$ ,  $IC_{50}$  p38 = 121.7 nM, Table 1), in which the trifluoromethyl group at the 2-position of the imidazole ring in KIN032 is replaced by phenyl mirrors the above observation that a larger group at the 2-position of the imidazole scaffold decreases the potency for B-Raf ( $IC_{50}$  B-Raf = 48.3 nM vs 21.4 nM) while increasing the potency for p38 $\alpha$  ( $IC_{50}$  p38 = 121.7 nM vs 405.2 nM). These observations are consis-

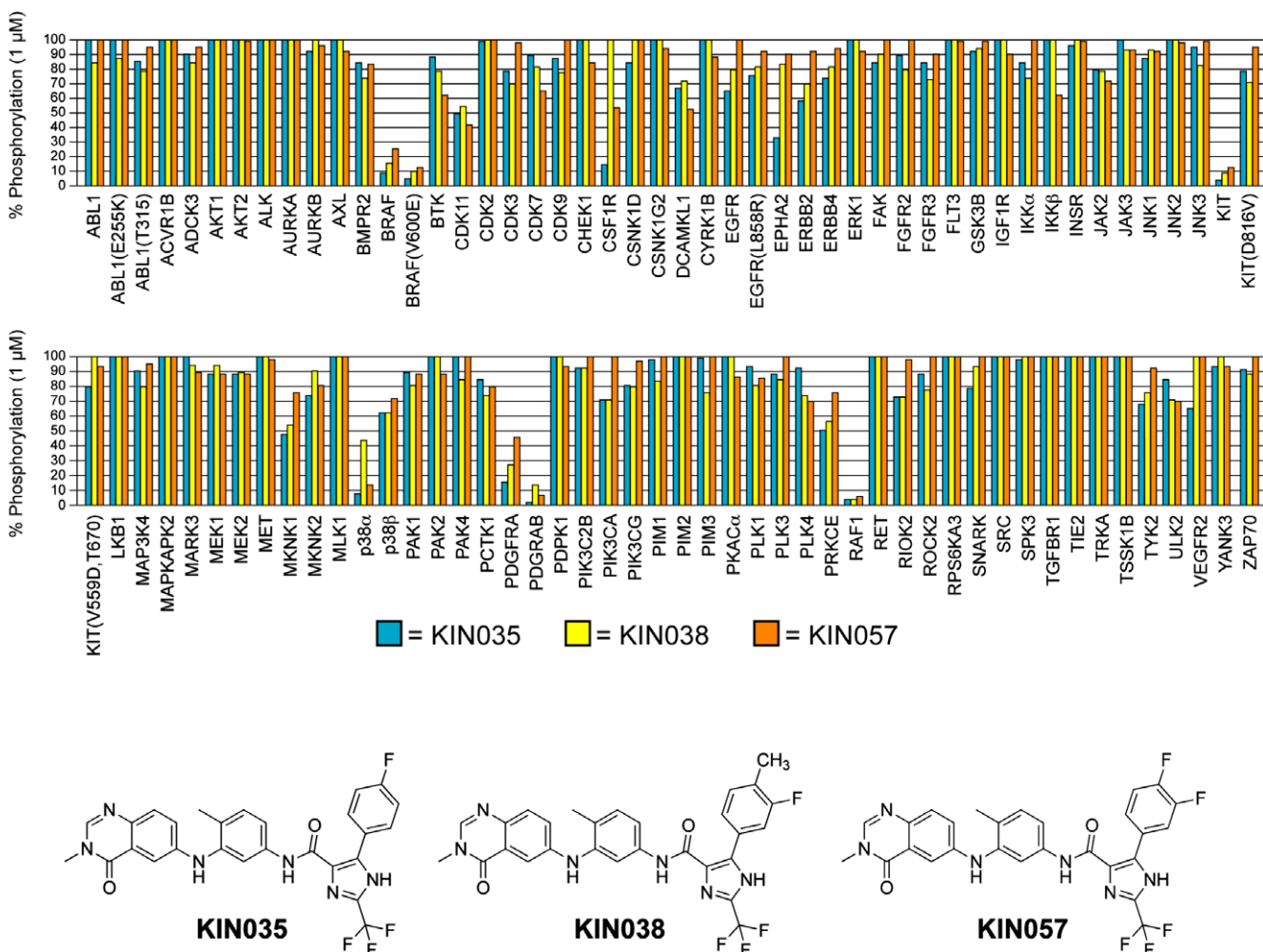


**Figure 7.** Kinase profiling results for KIN035, KIN038, KIN057. Molecules were assayed in duplicate at a 1  $\mu$ M concentration.

tent with the SAR trends reported for the BIRB-796 series of p38 $\alpha$  inhibitors at the lower selectivity pocket.<sup>29</sup>

The subnanomolar potency displayed by KIN035, KIN038, and KIN057 and the hypothesis that our molecules bound in a similar fashion as PLX4720, a molecule that shows decent selectivity for B-Raf V600E over wild type B-Raf,<sup>28</sup> led us to evaluate these three compounds in a B-Raf wild type assay. The results from this assay were very similar to the B-Raf V600E assay and displayed subnanomolar potency in the lower threshold or our assay conditions (1 nM B-Raf enzyme).

## 5. Kinase profiling

Three molecules, KIN035, KIN038, and KIN057 (Table 1, Fig. 7), were selected from the quinazolinone series to be evaluated for kinase profiling in 96 different kinases, including a separate assessment of all three molecules with respect to B-Raf V600E, at Ambit Bioscience Corporation (Ambit's protocol can be found in Ref. 30). Compounds were evaluated in duplicate at a single 1  $\mu$ M concentration. The selectivity profiles revealed that the quinazolinone series of compounds inhibited B-Raf and B-Raf V600E with near equal potency while also exhibiting varying degrees of c-Kit, p38 $\alpha$ , PDGFR-A, PDGFR-B, and C-Raf inhibition (Fig. 7). In agreement with in vitro data generated in our lab, KIN038 appeared selective for B-Raf kinase (Table 1, Fig. 7) over p38 $\alpha$ . Although the inhibitors reported here were not solely specific for B-Raf, they display a unique selectivity profile that is clearly different than that of sorafenib, which is now considered a broad spectrum kinase inhibitor. The kinase profile of Sorafenib has been published by Ambit Bioscience<sup>30</sup> and also described by others.<sup>19</sup> Sorafenib potently inhibits C-Raf, B-Raf, B-Raf V600E, VEGFR-1, VEGFR-2, VEGFR-3, PDGFR-B, Flt-3, Flt-4, p38, c-Kit, c-Abl, and FGFR-1.<sup>15</sup>

## 6. Conclusions

Structure-guided design methods combined with a chemocentric approach based on a novel chemistry entrance to tri-substituted imidazoles has been used to explore the binding requirements of the DFG-out allosteric form of B-Raf V600E mutant kinase. Proof of concept for this scaffold has been achieved through the incorporation of a previously reported quinazolinone hinge binding motif. Systematic exploration of the selectivity sites of B-Raf and p38 $\alpha$  kinase has resulted in the identification of KIN035, KIN038, and KIN057, which all display subnanomolar potency, tight inhibitor characteristics, and a unique kinase inhibition profile.

SAR studies generated from substitution on the phenyl ring located at the 5-position of the imidazole support our hypothesis that these molecules bind in a deep hydrophobic pocket and make specific interactions that are not typical of other known allosteric B-Raf inhibitors. Molecular modeling studies suggest that these inhibitors are capable of binding to a DFG-out form of B-Raf in a manner similar to that observed with PLX4720; however, the molecules reported here are hypothesized to utilize a significantly larger portion of the selectivity site in the DFG-out conformation of this enzyme. SAR generated here (Table 1 and Fig. 8) suggests the existence of a large and very hydrophobic upper selectivity pocket that can be exploited effectively. A fluorine substitution at either the 3 or 4 position of the phenyl ring located at the 5-position of the imidazole scaffold resulted in a dramatic increase in potency that may be associated with favorable edge-on interactions with the side chain of Phe468 and/or an increase in the polarity and hydrophobic character of the phenyl ring. Addition of a methyl substituent at the 4-position of the phenyl ring resulted in an increase in the selectivity over p38 $\alpha$  and is attributed to a steric interaction in p38 $\alpha$ .

The data reported here validates the 2,4,5-trisubstituted imidazole ring system as a core scaffold useful for inhibition of the DFG-out conformation of kinases. Ongoing efforts are aimed at the biological evaluation and, as necessary, improvements of the drug-like properties of these imidazole containing inhibitors through further modification of imidazole substituents and investigation of alternate hinge region motifs. In contrast to the massive screening of historical libraries, these studies illustrate how the seldom used exploration of versatile underutilized chemistry coupled with knowledge-based and structure-guided design efforts can provide truly new compounds, novel insights, and high value SAR in a very competitive area of research. Future reports will examine how this strategic chemocentric investment can be leveraged to construct high value, focused, compound libraries for not only kinases but other target classes as well.

## 7. Chemistry methods

<sup>1</sup>H NMR and <sup>13</sup>C NMR spectra were recorded on Bruker Avance spectrometer at 300 and 75 MHz, respectively, with TMS as an internal standard. HRMS experiments were performed on a Q-TOF-2TM (Micromass). TLC was performed with Merck 60 F254 silica gel plates. Column chromatography was performed using a Biotage SP1 system with manually loaded 12-, 25-, or 40-g columns. The purity of the target compounds was determined

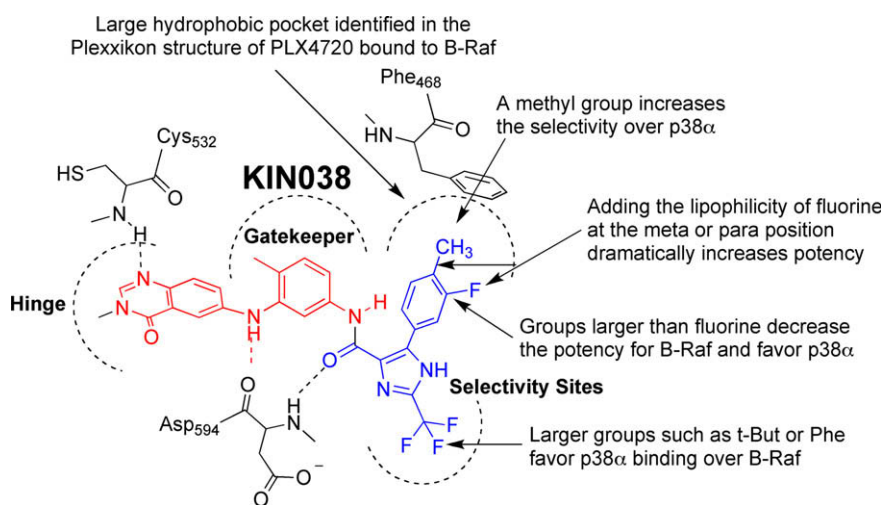


**Figure 8.** Two-dimensional schematic summary of SAR. The imidazole scaffold is shown in blue and the QUIN moiety is shown in red.

to be >95% by LC/MS on a Series 1100 LC/MSD (Agilent Technologies, Palo Alto, CA) equipped with a vacuum de-gasser (G1322A), a binary pump (1312A), an autosampler (G1313A), a thermostated column compartment (G1316A), and a mass selective detector (G1946A) supplied with atmospheric pressure ionization electrospray (API-ES). LC/MS utilized a Zorbax® C18 SB column (3.5  $\mu$ m, 4.6  $\times$  150 mm), MeCN/HOH/HAc (pH 4.8) elution buffer, and 15-min runs. Mass spectra and high resolution mass spectra were obtained using an ESI method by the Mass Spectroscopy Facility in the Chemistry Department at the University of Arizona. All solvents and reagents were purchased from Aldrich, TCI America, Matrix Scientific, and Ryan Scientific and used without further purification or drying.

## 8. Preparation of imidazole benzyl esters

### 8.1. General procedure

Phenyl glycine (1.0 g, 6.62 mmol) was added to a 25 mL round-bottomed flask that contained trifluoroacetic anhydride (3.0 mL) and stirred for 2 h at room temperature. Upon formation of oxazolinone, which was identified by TLC in 10% EtOAc/Hex ( $R_f$  = 0.70), excess TFAA and TFA were removed in vacuo as an azeotrope with toluene (5  $\times$  10 mL) at 60 °C. The remaining yellow solid was dissolved in 10 mL dry toluene and benzylcyanoformate (1.061 mL, 1.1 equiv, 7.28 mmol) was added via syringe followed by the dropwise addition of tributylphosphine (1.7 mL, 1 equiv, 6.63 mmol). CO<sub>2</sub> emission from the reaction was observed with an oil bubbler. The reaction was allowed to stir at room temperature for 12 h and then was concentrated to dryness under reduced pressure, dissolved in EtOAc, and washed with sodium bicarbonate, 1 M HCl, and brine. The crude mixture was purified on a Biotage sp1 system equipped with a 25 g silica column and eluted with a gradient of 5–60% EtOAc/Hex over 10 column volumes. Yields for this one-pot sequence ranged from 60% to 72%.

#### 8.1.1. Benzyl 5-phenyl-2-(trifluoromethyl)-1H-imidazole-4-carboxylate (5)

<sup>1</sup>H NMR (300 MHz, DMSO-*d*<sub>6</sub>):  $\delta$  14.5 (br s, 1H, NH), 7.68 (br s, 2H, Ar), 7.44 (br s, 3H, Ar), 7.33 (br s, 5H, Ar), 5.26 (s, 2H). ESMS:  $m/z$  347.2 [MH]<sup>+</sup>.

#### 8.1.2. Benzyl 5-*p*-tolyl-2-(trifluoromethyl)-1H-imidazole-4-carboxylate

<sup>1</sup>H NMR (300 MHz, DMSO-*d*<sub>6</sub>):  $\delta$  14.38 (br s, 1H, NH), 7.57 (d, 2H, Ar), 7.33 (br s, 5H, Ar), 7.23 (br s, 2H, Ar), 5.25 (s, 2H), 2.35 (s, 3H). ESMS:  $m/z$  [MH]<sup>+</sup>.

#### 8.1.3. Benzyl 5-(4-fluorophenyl)-2-(trifluoromethyl)-1H-imidazole-4-carboxylate

<sup>1</sup>H NMR (300 MHz, DMSO-*d*<sub>6</sub>):  $\delta$  14.35 (br s, 1H, NH), 7.71 (br s, 2H, Ar), 7.33 (br s, 5H, Ar), 7.26 (br s, 2H, Ar), 5.23 (s, 2H). ESMS:  $m/z$  365.2 [MH]<sup>+</sup>.

#### 8.1.4. Benzyl 5-(4-fluoro-3-methylphenyl)-2-(trifluoromethyl)-1H-imidazole-4-carboxylate

<sup>1</sup>H NMR (300 MHz, DMSO-*d*<sub>6</sub>):  $\delta$  14.40 (br s, 1H, NH), 7.54–7.61 (m, 2H, Ar), 7.33 (br s, 5H, Ar), 7.18 (t, 1H,  $J$  = 9.0 Hz, Ar), 5.25 (s, 2H), 2.21 (s, 3H). ESMS:  $m/z$  379.2 [MH]<sup>+</sup>.

#### 8.1.5. Benzyl 5-(3-fluoro-4-methylphenyl)-2-(trifluoromethyl)-1H-imidazole-4-carboxylate

<sup>1</sup>H NMR (300 MHz, DMSO-*d*<sub>6</sub>):  $\delta$  12.50 (br s, 1H, NH), 7.10–7.83 (m, 8H) 5.24 (s, 2H), 2.29 (s, 3H). ESMS:  $m/z$  379.2 [MH]<sup>+</sup>.

#### 8.1.6. Benzyl 5-(3-chloro-4-fluorophenyl)-2-(trifluoromethyl)-1H-imidazole-4-carboxylate

<sup>1</sup>H NMR (300 MHz, DMSO-*d*<sub>6</sub>):  $\delta$  14.60 (br s, 1H, NH), 7.97 (d, 1H,  $J$  = 6.0 Hz, Ar), 7.73 (s, 1H, Ar), 7.46 (dd, 1H,  $J$  = 6 Hz), 7.35 (br s, 5H, Ar), 5.27 (s, 2H). ESMS:  $m/z$  399.2 [MH]<sup>+</sup>.

#### 8.1.7. Benzyl 2-(trifluoromethyl)-5-(3,4,5-trimethoxyphenyl)-1H-imidazole-4-carboxylate

<sup>1</sup>H NMR (300 MHz, DMSO-*d*<sub>6</sub>):  $\delta$  14.30 (br s, 1H, NH), 7.33 (br s, 5H, Ar), 7.01 (s, 2H, Ar), 5.26 (s, 2H), 3.74 (s, 6H), 3.71 (s, 3H). ESMS:  $m/z$  437.2 [MH]<sup>+</sup>.

#### 8.1.8. Benzyl 2-(trifluoromethyl)-5-(3-(trifluoromethyl)phenyl)-1H-imidazole-4-carboxylate

<sup>1</sup>H NMR (300 MHz, DMSO-*d*<sub>6</sub>):  $\delta$  14.5 (br s, 1H, NH), 8.10 (br s, 1H, Ar), 8.03 (br s, 1H, Ar), 7.79 (br s, 1H, Ar), 7.66 (m, 1H), 7.33 (br s, 5H, Ar), 5.28 (s, 2H). ESMS:  $m/z$  415.2 [MH]<sup>+</sup>.

#### 8.1.9. Benzyl 2-(trifluoromethyl)-5-(2-(trifluoromethyl)phenyl)-1H-imidazole-4-carboxylate

<sup>1</sup>H NMR (300 MHz, DMSO-*d*<sub>6</sub>):  $\delta$  14.6 (br s, 1H, NH), 7.66–7.84 (m, 4H, Ar), 7.26 (m, 3H,  $J$  = 2.0 Hz,  $J$  = 5.1 Hz), 6.98 (m, 2H, Ar), 5.08 (br s, 2H, Ar). ESMS:  $m/z$  415.2 [MH]<sup>+</sup>.

#### 8.1.10. Benzyl 5-(3,4-difluorophenyl)-2-(trifluoromethyl)-1H-imidazole-4-carboxylate

<sup>1</sup>H NMR (300 MHz, DMSO-*d*<sub>6</sub>):  $\delta$  14.5 (br s, 1H, NH), 7.83 (m, 1H, Ar), 7.46–7.60 (m, 2H, Ar), 7.35 (br s, 5H, Ar), 5.28 (s, 2H).

#### 8.1.11. Methyl 2-*tert*-butyl-5-*p*-tolyl-1H-imidazole-4-carboxylate

<sup>1</sup>H NMR (300 MHz, DMSO-*d*<sub>6</sub>):  $\delta$  12.8 and 11.8 (br s, 1H, taut), 8.02 (d, 2H,  $J$  = 7.8 Hz), 7.26 (d, 2H,  $J$  = 7.8 Hz), 3.83 and 3.75 (s, 3H), 2.36 (s, 3H), 1.44 and 1.39 (s, 9H, taut).

#### 8.1.12. 2-Benzamido-2-phenylacetic acid

2.0 M NaOH (50 mL) and phenyl glycine (3.0 g, 19.85 mmol) was added to a 250 mL round-bottomed flask equipped with a magnetic stirrer. This solution was cooled to 0 °C on an ice bath, and then benzoyl chloride (3.07 g, 1.1 equiv, 21.83 mmol) was added dropwise over the course of 20 min. The reaction was allowed to warm to room temperature and then proceeded for 2 h. The solution was made slightly acidic (pH 5–6) by the dropwise addition of 2.0 M HCl and was extracted into EtOAc (5  $\times$  75 mL), which was dried over magnesium sulfate and concentrated to yield 4.76 g (94% yield) of phenylglycine phenylacetamide. <sup>1</sup>H NMR (300 MHz, DMSO-*d*<sub>6</sub>):  $\delta$  13.0 (br s, 1H, OH), 9.07 (d, 1H,  $J$  = 7.5 Hz, N-H), 7.93 (d, 2H,  $J$  = 6.9 Hz, Ar), 7.29–7.64 (m, 8H), 5.64 (d, 1H,  $J$  = 7.5 Hz).

#### 8.1.13. 2,4-Diphenyloxazol-5(4H)-one

Phenylglycine phenylacetamide (4.5 g, 17.63 mmol) and 15 mL dry DCM was added to a 50 mL round-bottomed flask with magnetic stirrer followed by the dropwise addition of acetic anhydride (3.3 mL). This reaction was allowed to proceed for 2 h upon which time it was placed in a separatory funnel that contained 50 mL sodium bicarbonate. Oxazolinone was extracted into DCM (2  $\times$  75 mL), dried over magnesium sulfate, and concentrated in vacuo to yield 3.4 g 1,4-diphenyl oxazolinone as a light yellow solid (3.4 g, 14.33 mmol, 81% yield)  $R_f$  = 0.70, 15% EtOAc/Hex.

#### 8.1.14. Benzyl 2,5-diphenyl-1H-imidazole-4-carboxylate (tautomers)

Benzylcyanoformate (1.014 mL, 1.1 equiv, 6.95 mmol) was added to a 25 mL round-bottomed flask with 10 mL dry toluene and diphenyl oxazolinone (1.5 g, 6.32 mmol) followed by the drop-

wise addition of tributylphosphine (0.390 mL, 0.25 equiv, 1.581 mmol). An oil bubbler was attached to the reaction vessel to observe CO<sub>2</sub> emission from the reaction. The reaction was allowed to react for 14 h and then concentrated to dryness under reduced pressure, dissolved in EtOAc, and washed with sodium bicarbonate, 1 M HCl, and brine. The crude mixture was purified on a Biotage sp1 system equipped with a 25-g silica column and eluted with a gradient of 5–60% EtOAc/Hex over 10 CV to yield 1.34 g product (80.0% yield, 5.06 mmol). <sup>1</sup>H NMR (300 MHz, DMSO-*d*<sub>6</sub>): δ 13.1 and 13.3 (br s, 1H, NH), 8.21 (d, 1H, *J* = 6.8 Hz), 8.07 (d, 1H, *J* = 7.1 Hz), 7.86 (d, 1H, *J* = 3.5 Hz), 7.45–7.55 (m, 5H, Ar), 7.30–7.40 (m, 6H), (5.34 and 5.24) (s, 2H). ESMS: *m/z* 355.2 [MH]<sup>+</sup>.

## 9. Synthesis of imidazole carboxylic acids

### 9.1. General procedure

Imidazole benzyl ester (750 mg) was dissolved in approximately 30 mL MeOH in a Parr hydrogenation bottle. Argon was bubble through for 5 min and then 100 mg 10% Pd/C was added. The bottle was shaken on a Parr hydrogenation apparatus for 2 h upon which the reaction was complete as observed by TLC (*R*<sub>f</sub> = .01, 30% EtOAc/Hex). The mixture was filtered through Celite followed by the addition of 20 mL DCM. The solvent was then concentrated in vacuo and solids dried in a vacuum oven at 60 °C to yield the imidazole carboxylic acid in 94–98% yield.

#### 9.1.1. 5-Phenyl-2-(trifluoromethyl)-1*H*-imidazole-4-carboxylic acid (10)

<sup>1</sup>H NMR (300 MHz, DMSO-*d*<sub>6</sub>): δ 14.2 (br s, 1H), 13.2 (br s, 1H), 7.78 (br s, 2H), 7.45 (m, 3H). <sup>13</sup>C NMR (75 MHz, DMSO-*d*<sub>6</sub>): δ 163.05 (br), 145.90 (br), 139.89 (br), 130.288 (2C), 129.18, 128.23 (2C), 122.42 (br), 119.34 (q, 1C, *J* = 269.5 Hz). ESMS: *m/z* 257.2 [MH]<sup>+</sup>.

#### 9.1.2. 5-*p*-Tolyl-2-(trifluoromethyl)-1*H*-imidazole-4-carboxylic acid

<sup>1</sup>H NMR (300 MHz, DMSO-*d*<sub>6</sub>): δ 13.0–15.0 (br s, 2H), 7.65 (br s, 2H), 7.25 (d, 2H, *J* = 8.0 Hz). <sup>13</sup>C NMR (75 MHz, DMSO-*d*<sub>6</sub>): δ 163.54 (br), 146.32 (br), 139.17, 136.28 (br), 130.15, 129.31 (2C), 123.62 (br), 119.36 (q, 1C, *J* = 268.0 Hz). ESMS: *m/z* 271.2 [MH]<sup>+</sup>.

#### 9.1.3. 5-(4-Fluorophenyl)-2-(trifluoromethyl)-1*H*-imidazole-4-carboxylic acid

<sup>1</sup>H NMR (300 MHz, DMSO-*d*<sub>6</sub>): δ 13.3 (br s, 1H), 7.86 (dd, 2H, *J* = 5.7 Hz, *J* = 8.35), 7.25 (tt, 2H, *J* = 11.8 Hz, *J* = 2.8 Hz). <sup>13</sup>C NMR (75 MHz, DMSO-*d*<sub>6</sub>): δ 163.13 (d, 4-F Ar, *J* = 244.5), 162.76 (br, C=O), 142.49 (br), 136.28 (q, *J* = 40.8), 132.44 (d, 2C, 2,6 Ar, *J* = 8.4 Hz), 128.23 (br), 125.84 (br), 119.32 (q, 1C, *J* = 267.9 Hz), 115.62 (d, 2C, 3,5-Ar, *J* = 21.5 Hz). ESMS: *m/z* 275.2 [MH]<sup>+</sup>.

#### 9.1.4. 5-(4-Fluoro-3-methylphenyl)-2-(trifluoromethyl)-1*H*-imidazole-4-carboxylic acid

<sup>1</sup>H NMR (300 MHz, acetone-*d*<sub>6</sub>): δ 11.0–13.0 (br s, 1H), 7.84 (d, 1H, *J* = 6.2 Hz), 7.79 (s, 1H), 7.13 (t, 1H, *J* = 9.4 Hz), 2.31 (s, 3H). <sup>13</sup>C NMR (75 MHz, DMSO-*d*<sub>6</sub>): δ 161.95 (d, 4-F Ar, *J* = 244.5), 162.45 (br, C=O), 142.40 (br), 136.28 (q, *J* = 40.8), 133.15 (d, *J* = 5.3 Hz), 129.42 (d, *J* = 8.4 Hz), 123.50 (br), 124.52 (d, *J* = 17.6 Hz), 118.98 (q, 1C, *J* = 267.5 Hz), 13.97 (d, *J* = 3.5 Hz). ESMS: *m/z* 289.2 [MH]<sup>+</sup>.

#### 9.1.5. 5-(3-Fluoro-4-methylphenyl)-2-(trifluoromethyl)-1*H*-imidazole-4-carboxylic acid

<sup>1</sup>H NMR (300 MHz, acetone-*d*<sub>6</sub>): δ 14.0 (br s, 1H), 7.64 (d, 1H, *J* = 11.0 Hz), 7.57 (s, 1H), 7.34 (t, 1H, *J* = 7.9 Hz), 2.28 (s, 3H). <sup>13</sup>C

NMR (75 MHz, DMSO-*d*<sub>6</sub>): δ 162.46, 160.86 (d, *J* = 240.0 Hz), 143.30 (br), 136.4 (q, 39.0 Hz), 131.90 (d, *J* = 5.3 Hz), 129.50, 125.89, 125.13, 119.25 (q, *J* = 268.0 Hz), 116.51 (d, *J* = 25.4 Hz), 14.86 (d, *J* = 3.0 Hz). ESMS: *m/z* 289.2 [MH]<sup>+</sup>.

#### 9.1.6. 2-(Trifluoromethyl)-5-(3-(trifluoromethyl)phenyl)-1*H*-imidazole-4-carboxylic acid

<sup>1</sup>H NMR (300 MHz, DMSO-*d*<sub>6</sub>): δ 13.0–14.0 (br s, 1H), 8.21 (s, 1H), 8.14 (d, 1H, *J* = 7.7 Hz), 7.77 (d, 1H, *J* = 7.8 Hz), 7.68 (t, 1H, *J* = 7.7 Hz). <sup>13</sup>C NMR (75 MHz, DMSO-*d*<sub>6</sub>): δ 162.40 (C=O), 142.25, 136.82 (q, *J* = 39.9 Hz), 134.07 (Ar), 133.11 (br), 129.86 (Ar), 129.60 (q, *J* = 31.7, Ar), 126.62 (q, 3.9 Hz, Ar), 125.93 (q, Ar), 125.81 (q, *J* = 272.3 Hz, CF<sub>3</sub>), 120.012 (q, *J* = 269.8 Hz, CF<sub>3</sub>). ESMS: *m/z* 325.2 [MH]<sup>+</sup>.

#### 9.1.7. 2-(Trifluoromethyl)-5-(2-(trifluoromethyl)phenyl)-1*H*-imidazole-4-carboxylic acid

<sup>1</sup>H NMR (300 MHz, DMSO-*d*<sub>6</sub>): δ 13.0–14.0 (br s, 1H), 7.85 (d, 1H, *J* = 7.0 Hz), 7.66–7.77 (m, 2H, *J* = 7.2 Hz), 7.57 (d, 1H, *J* = 7.1 Hz). <sup>13</sup>C NMR (75 MHz, DMSO-*d*<sub>6</sub>): δ 162.40 (C=O), 136.02 (q, *J* = 39.5 Hz), 133.45 (Ar), 132.78 (Ar), 130.44 (Ar), 129.03 (q, *J* = 129.7 Hz, Ar), 126.72 (q, *J* = 4.9 Hz, Ar), 124.64 (q, *J* = 273.8 Hz, CF<sub>3</sub>), 119.31 (q, *J* = 269.6 Hz, CF<sub>3</sub>). ESMS: *m/z* 325.2 [MH]<sup>+</sup>.

#### 9.1.8. 2-(Trifluoromethyl)-5-(3,4,5-trimethoxyphenyl)-1*H*-imidazole-4-carboxylic acid

<sup>1</sup>H NMR (300 MHz, DMSO-*d*<sub>6</sub>): δ 13.0–14.0 (br s, 1H), 7.19 (s, 2H), 3.81 (s, 6H), 3.72 (s, 3H). <sup>13</sup>C NMR (75 MHz, DMSO-*d*<sub>6</sub>): δ 163.20 (C=O), 153.14 (2C, Ar), 148.18, 138.88, 135.66 (q, *J* = 39.5 Hz), 127.0 (br), 119.35 (q, *J* = 267.6 Hz), 115.86, 107.89, 60.930 (OMe), 56.79 (2C, OMe) 133.45 (Ar), 132.78 (Ar), 130.44 (Ar), 129.03 (q, *J* = 129.7 Hz, Ar), 126.72 (q, *J* = 4.9 Hz, Ar), 124.64 (q, *J* = 273.8 Hz, CF<sub>3</sub>), 119.31 (q, *J* = 269.6 Hz, CF<sub>3</sub>). ESMS: *m/z* 347.2 [MH]<sup>+</sup>.

#### 9.1.9. 5-(3-Chloro-4-fluorophenyl)-2-(trifluoromethyl)-1*H*-imidazole-4-carboxylic acid

<sup>1</sup>H NMR (300 MHz, acetone-*d*<sub>6</sub>): δ 14.5 (br s, 1H), 13.5 (br s, 1H), 7.95 (m, 1H), 7.71 (s, 1H), 7.50 (dd, 1H, *J* = 9.0 Hz, *J* = 18.6 Hz). <sup>13</sup>C NMR (75 MHz, acetone-*d*<sub>6</sub>): δ 161.46 (br), 158.39 (d, *J* = 248.0 Hz), 143.40 (br), 136.76 (q), 131.88, 130.32 (d, *J* = 7.42), 120.13 (d, *J* = 17.78 Hz), 118.86 (q, *J* = 267.7 Hz), 116.56 (d, 13.73 Hz), 114.6 (br). ESMS: *m/z* 309.2 [MH]<sup>+</sup>.

#### 9.1.10. 2-*tert*-Butyl-5-*p*-tolyl-1*H*-imidazole-4-carboxylic acid

<sup>1</sup>H NMR (300 MHz, DMSO-*d*<sub>6</sub>): δ 12.23 (br s, 1H), 7.71 (br s, 2H), 7.19 (d, 2H (br s, 2H, *J* = 7.8 Hz), 2.32 (s, 3H), 1.34 (s, 9H). <sup>13</sup>C NMR (75 MHz, acetone-*d*<sub>6</sub>): δ 162.69, 158.13, 145.26, 137.74, 132.43, 129.93 (2C), 128.98 (2C), 118.72, 33.61, 30.00, 21.73. ESMS: *m/z* 259.2 [MH]<sup>+</sup>.

#### 9.1.11. 2,5-Diphenyl-1*H*-imidazole-4-carboxylic acid

<sup>1</sup>H NMR (300 MHz, DMSO-*d*<sub>6</sub>): δ 13.0–14.0 (br s, 1H), 7.2–8.3 (br m, 10H). <sup>13</sup>C NMR (75 MHz, DMSO-*d*<sub>6</sub>): δ 162.28, 148.168, 147.368, 134.87, 133.46, 130.34, 130.02, 129.54, 128.51, 128.13, 127.13, 126.50, 120.55. ESMS: *m/z* 265.2 [MH]<sup>+</sup>.

#### 9.1.12. 5-(3,4-Difluorophenyl)-2-(trifluoromethyl)-1*H*-imidazole-4-carboxylic acid

<sup>1</sup>H NMR (300 MHz, acetone-*d*<sub>6</sub>): δ 14.5 (br s, 1H), 13.5 (br s, 1H), 7.95 (m, 1H), 7.71 (s, 1H), 7.50 (dd, 1H, *J* = 9.0 Hz, *J* = 18.6 Hz). <sup>13</sup>C NMR (75 MHz, acetone-*d*<sub>6</sub>): δ 161.62 (br), 150.42 (dd, *J* = 10.7 Hz, *J* = 244.6 Hz), 149.62 (dd, *J* = 11.8 Hz, *J* = 243.4 Hz), 143.71 (br), 136.73 (br), 130.64 (br), 127.16 (m), 122.89 (br) 119.24 (m),

119.18 (q,  $J = 269.8$ ), 117.90 (d,  $J = 17.3$  Hz). ESMS:  $m/z$  293.2 [MH]<sup>+</sup>.

#### 9.1.13. Synthesis of 6-(5-amino-2-methylphenylamino)-3-methylquinazolin-4(3H)-one *tert*-butyl 4-methyl-3-nitrophenylcarbamate

A solution of 4-methyl-3-nitroaniline (15.0 g, 99 mmol) was dissolved in 50 mL THF at 65 °C. 25.8 g Boc anhydride was dissolved in 30 mL THF and added dropwise over the course of 20 min. The reaction was refluxed overnight, cooled to room temperature, and then concentrated in vacuo to yield a brown oil. The oil was dissolved in 150 mL 20% EtOAc/Hex and 50 g of silica gel was added. The solution was stirred for 15 min on a rotovap and the silica was removed by filtration and washed with 300 mL 20% EtOAc/Hex. The organics were dried over magnesium sulfate and then concentrated by vacuum filtration to yield 20.7 g product in 83% yield. <sup>1</sup>H NMR (300 MHz, DMSO-*d*<sub>6</sub>):  $\delta$  9.75 (br s, 1H), 8.22 (d, 1H,  $J = 2.1$  Hz), 7.58 (dd, 1H,  $J = 2.1$  Hz,  $J = 8.3$  Hz), 7.37 (d, 1H,  $J = 8.3$  Hz), 2.43 (s, 3H), 1.48 (s, 9H). <sup>13</sup>C NMR (75 MHz, DMSO-*d*<sub>6</sub>):  $\delta$  153.50, 148.48, 139.45, 133.79, 126.65, 123.52, 113.81, 80.60, 28.84, 19.92. ESMS:  $m/z$  270.0 [M+H<sub>2</sub>O].

#### 9.1.14. *tert*-Butyl 3-amino-4-methylphenylcarbamate

*tert*-Butyl 4-methyl-3-nitrophenylcarbamate (20.7 g, 82.0 mmol) was dissolved in 200 mL EtOH and 1.0 g of 5% Pd/C was added. The mixture was hydrogenated on a Parr system at 50 PSI hydrogen for 15 h. Completion of reaction was shown by TLC in 30% EtOAc/Hex, then filtered, concentrated, and dried in a vacuum oven to yield the product (16.78 g, 75.0 mmol, 92% yield). <sup>1</sup>H NMR (300 MHz, DMSO-*d*<sub>6</sub>):  $\delta$  8.93 (br s, 1H), 6.85 (s, 1H), 6.75 (d, 1H,  $J = 8.0$  Hz), 6.5 (d, 1H,  $J = 8.0$  Hz), 4.75 (s, 2H), 1.97 (s, 3H), 1.46 (s, 9H). <sup>13</sup>C NMR (75 MHz, DMSO-*d*<sub>6</sub>):  $\delta$  153.58, 147.37, 138.777, 130.51, 115.87, 107.53, 105.07, 79.20, 29.05, 17.71. ESMS:  $m/z$  223.2 [MH]<sup>+</sup>.

#### 9.1.15. 6-Chloro-3-methylquinazolin-4(3H)-one

2-Amino-5-chlorobenzoic acid (12.5 g, 73 mmol) was placed in a 250 mL beaker containing *N*-methylformamide (125 mL). A condenser was utilized, and the reaction was heated overnight at 180 °C. The reaction was complete the next morning and allowed to cool to room temperature for 1 h and then poured into 500 mL of water and extracted three times with 250 mL of ethyl acetate. The organic phase was then washed with an additional 1 l of water and concentrated under vacuum to yield 6-chloro-3-methylquinazolin-4(3H)-one (9.2 g, 47.3 mmol, 65% yield). <sup>1</sup>H NMR (300 MHz, DMSO-*d*<sub>6</sub>):  $\delta$  8.39 (s, 1H), 8.04 (d, 1H,  $J = 3.6$  Hz), 7.82 (dd, 1H,  $J = 2.4$  Hz,  $J = 8.7$  Hz), 7.67 (1H, d,  $J = 8.7$  Hz), 3.49 (s, 3H). <sup>13</sup>C NMR (75 MHz, DMSO-*d*<sub>6</sub>):  $\delta$  160.49, 149.75, 147.65, 135.06, 131.99, 130.26, 125.61, 123.45, 34.53. ESMS:  $m/z$  195.2 [MH]<sup>+</sup>.

#### 9.1.16. *tert*-Butyl 4-methyl-3-(3-methyl-4-oxo-3,4-dihydroquinazolin-6-ylamino)phenylcarbamate

To refluxing toluene (50 mL) in a 150 mL round-bottomed flask was added 2-methyl-5-*t*-butylcarbamate aniline (3 g, 13.50 mmol, 1.2 equiv), 6-chloro-3-methyl-4-oxoquinazolinone (2.19 g, 11.25 mmol, 1 equiv), NaOMe (1.51 g, 15.75 mmol, 1.4 equiv), 2-diphenylbistbutylphosphine (168 mg, 5 mol %, 0.561 mmol), and Pd<sub>2</sub>(dba)<sub>3</sub> (309 mg, 3 mol %, 0.336 mmol). This mixture was refluxed for 8 h when it was observed there was complete amination of quinazolinone starting material. The reaction mixture was cooled to room temperature and poured into 250 mL EtOAc and then washed with sodium bicarbonate (2 × 100 mL), water (2 × 100 mL), and then brine (2 × 100 mL). The light brown solid was then purified by flash chromatography on silica (70% EtOAc/

Hex) to yield desired product as a light yellow solid (3.6 g, 9.33 mmol, 83% yield). <sup>1</sup>H NMR (300 MHz, DMSO-*d*<sub>6</sub>):  $\delta$  7.91 (s, 1H), 7.64 (d, 1H,  $J = 2.7$  Hz), 7.61 (s, 1H,  $J = 8.8$  Hz), 7.34 (dd, 1H,  $J = 2.7$  Hz,  $J = 8.8$  Hz), 7.29 (s, 1H), 7.16 (d, 1H,  $J = 8.2$  Hz), 7.09 (d, 1H,  $J = 8.2$  Hz), 6.47 (s, 1H), 5.70 (s, 1H), 3.59 (s, 3H), 1.64 (s, 3H), 1.51 (s, 9H). <sup>13</sup>C NMR (75 MHz, DMSO-*d*<sub>6</sub>):  $\delta$  161.34, 153.57, 145.59, 145.58, 141.04, 139.09, 131.84, 129.01, 125.35, 123.96, 123.24, 114.31, 112.49, 108.33, 79.70, 34.26, 28.97, 18.14. ESMS:  $m/z$  381.2 [MH]<sup>+</sup>.

#### 9.1.17. 6-(5-Amino-2-methylphenylamino)-3-methylquinazolin-4(3H)-one

*tert*-Butyl 4-methyl-3-(3-methyl-4-oxo-3,4-dihydroquinazolin-6-ylamino)phenylcarbamate (3.0 g, 7.89 mmol) was added to 50 mL of 10% TFA in DCM. After 1 h, the reaction mixture was neutralized with 75 mL saturated Na<sub>2</sub>CO<sub>3</sub>, extracted into EtOAc (3 × 100 mL), dried over MgSO<sub>4</sub> and concentrated in vacuo to yield the desired product (2.078 g, 7.41 mmol, 94% yield). <sup>1</sup>H NMR (300 MHz, DMSO-*d*<sub>6</sub>):  $\delta$  7.91 (s, 1H), 7.71 (d, 1H,  $J = 2.7$  Hz), 7.61 (s, 1H,  $J = 8.8$  Hz), 7.37 (dd, 1H,  $J = 2.7$  Hz,  $J = 8.8$  Hz), 7.31 (s, 1H), 7.03 (d, 1H,  $J = 8.0$  Hz), 6.67 (d, 1H,  $J = 2.3$  Hz), 6.40 (dd, 1H,  $J = 2.4$  Hz,  $J = 8.0$  Hz), 5.80 (br s, 1H), 3.63 (s, 3H), 2.16 (s, 3H), 1.64 (s, 3H), 1.51 (s, 9H). <sup>13</sup>C NMR (75 MHz, DMSO-*d*<sub>6</sub>):  $\delta$  160.73, 146.90, 144.88, 142.13, 138.84, 132.85, 131.08, 130.76, 126.96, 125.08, 122.78, 118.25, 115.49, 110.06, 34.87, 18.51. ESMS:  $m/z$  281.2 [MH]<sup>+</sup>.

## 10. Preparation of imidazole-quinazolinones

### 10.1. General method 10.1.1. *N*-(4-Methyl-3-(3-methyl-4-oxo-3,4-dihydroquinazolin-6-ylamino)phenyl)-5-phenyl-2-(trifluoromethyl)-1H-imidazole-4-carboxamide (KIN032)

In a 20 mL vial equipped with a magnetic stirrer and DCM (3 mL) at 0 °C was added the corresponding imidazole acid (75 mg, 0.293 mmol, 1 equiv), EDCI (84 mg, 1.5 equiv, 0.439 mmol), HOAt (86 mg, 1.3 equiv, 0.381 mmol), DIPEA (210  $\mu$ L, 4 equiv, 1.171 mmol). This solution was allowed to react for 1 h at 0 °C and then amine (82 mg, 1 equiv, 0.293 mmol) was added. The reaction was allowed to react for 24 h at which time it was added to 50 mL saturated sodium bicarbonate and extracted into 100 mL EtOAc. The organic layer was washed with water (30 mL) and brine (30 mL), dried over magnesium sulfate, and concentrated onto silica. Final compound was purified on a Biotage SP1 system utilizing a 25-g silica column and a gradient of 2–8% MeOH/CHCl<sub>3</sub> to yield the desired product (83 mg, 1.86 mmol, 54.7% yield).  $R_f = 0.42$  in 5% MeOH/CHCl<sub>3</sub>. <sup>1</sup>H NMR (300 MHz, CDCl<sub>3</sub>-*d*<sub>6</sub>):  $\delta$  12.05 (br s, 1H), 9.07 (br s, 1H), 7.78 (m, 2H), 7.50 (m, 4H), 7.28 (m, 2H), 7.18 (m, 5H), 3.36 (s, 3H), 2.19 (s, 3H). <sup>13</sup>C NMR (75 MHz, CDCl<sub>3</sub>-*d*<sub>6</sub>):  $\delta$  162.00, 147.32, 144.63, 144.06, 142.06, 140.23, 137.24, 135.38 (q,  $J = 41.7$  Hz), 131.77, 131.29, 129.68 (2C), 129.59, 128.92, 128.30, 126.67, 124.35, 123.11, 120.63 (q,  $J = 268.0$  Hz), 115.96, 113.12, 109.92, 39.12, 14.44. LC/MS 96.54%, [M]<sup>−</sup> = 517.2. HRMS (ESI) (M+1): 519.1751 calcd for C<sub>27</sub>H<sub>21</sub>F<sub>3</sub>N<sub>6</sub>O<sub>2</sub> (M+1): 519.1678.

### 10.1.2. *N*-(4-Methyl-3-(3-methyl-4-oxo-3,4-dihydroquinazolin-6-ylamino)phenyl)-5-*p*-tolyl-2-(trifluoromethyl)-1H-imidazole-4-carboxamide (KIN031)

<sup>1</sup>H NMR (300 MHz, 30% MeOD/CDCl<sub>3</sub>): 7.78 (s, 1H), 7.40–7.48 (m, 3H), 7.37 (d, 1H,  $J = 8.8$  Hz), 7.35 (d, 1H,  $J = 2.4$  Hz), 7.24 (d, 1H,  $J = 2.6$  Hz), 7.21 (d, 1H,  $J = 2.8$  Hz), 7.04–7.09 (m, 3H), 3.42 (s, 3H), 2.22 (s, 3H), 2.06 (s, 2H). <sup>13</sup>C NMR (75 MHz, 30% MeOD/CDCl<sub>3</sub>): 162.10, 160.71, 145.44, 144.07, 140.99, 140.21, 139.67, 130.06, 136.88, 135.00 (q, 40.3 Hz), 131.65, 130.74, 129.51, 129.06, 128.16, 127.54, 125.54, 123.88, 122.87, 118.66 (q,  $J = 269.3$  Hz),

116.19, 114.05, 109.10, 34.28, 21.38, 17.57  $\delta$  LC/MS 100.0%,  $[M]^- = 531.2$   $t_R = 7.62$  min. HRMS (ESI) (M+1): 533.1907 calcd for  $C_{28}H_{23}F_3N_6O_2$  (M+1): 533.1835.

**10.1.3. 5-(4-Fluorophenyl)-N-(4-methyl-3-(3-methyl-4-oxo-3,4-dihydroquinazolin-6-ylamino)phenyl)-2-(trifluoromethyl)-1H-imidazole-4-carboxamide (KIN035)**

$^1H$  NMR (300 MHz, acetone- $d_6$ ):  $\delta$  13.0 (br s, 1H, imid NH), 9.58 (br s, 1H, NH), 8.06 (s, 1H, Ar), 7.93–7.98 (m, 3H), 7.60 (d, 1H,  $J = 2.5$  Hz), 7.45–7.56 (m, 3H), 7.33 (s, 1H), 7.19–7.26 (m, 3H).  $^{13}C$  NMR (75 MHz, acetone- $d_6$ ):  $\delta$  162.62 (d,  $J = 379$  Hz), 161.86, 161.09, 145.06, 144.92, 142.25, 141.14, 138.11, 136.40, 134.33 (q,  $J = 41.1$  Hz), 132.35 (d, 2C,  $J = 12.5$  Hz), 131.90 (br), 131.48, 128.84, 126.37, 125.25 (br), 123.86, 123.43, 119.02, 115.39 (d, 2C,  $J = 2.1$  Hz), 115.08, 113.15, 109.39, 30.34, 17.25. LC/MS 96.44%  $t_R = 8.36$  min  $[M]^- = 535.2$ . HRMS = 536.1657 calcd HRMS = 536.1584. 51.2% yield.

**10.1.4. 5-(4-Fluoro-3-methylphenyl)-N-(4-methyl-3-(3-methyl-4-oxo-3,4-dihydroquinazolin-6-ylamino)phenyl)-2-(trifluoromethyl)-1H-imidazole-4-carboxamide (KIN037)**

$^1H$  NMR (300 MHz, acetone- $d_6$ ):  $\delta$  13.0 (br s, 1H, imid NH), 9.58 (br s, 1H, NH), 8.11 (s, 1H, Ar), 7.95 (s, 1H), 7.77 (s, 1H), 7.51 (m, 1H), 7.60 (d, 1H,  $J = 2.5$  Hz), 7.56 (d, 1H,  $J = 8.8$  Hz), 7.52 (m, 1H), 7.49 (dd, 1H,  $J = 8.8$  Hz,  $J = 2.5$  Hz), 7.35 (s, 1H), 7.24 (d,  $J = 8.2$  Hz), 7.118 (t, 1H,  $J = 9.3$  Hz), 3.53 (s, 3H), 2.59 (d, 3H,  $J = 3.6$  Hz), 2.59 (s, 3H).  $^{13}C$  NMR (75 MHz, acetone- $d_6$ ):  $\delta$  161.121, 160.195 (d,  $J = 242.2$  Hz), 145.04, 144.90, 142.22, 141.16, 138.08, 136.26, 134.43 (q,  $J = 41.6$  Hz), 131.98, 131.49 (d,  $J = 5.3$  Hz), 149.485, 128.79, 128.37 (d,  $J = 9.7$  Hz), 126.35, 126.20 (d,  $J = 17.2$ ), 125.42 (d,  $J = 3.3$  Hz), 123.91, 123.40, 119.00 (q,  $J = 268.8$  Hz), 116.60 (d,  $J = 25.0$  Hz), 115.40, 113.01, 109.463, 33.35, 17.25, 13.92 (d,  $J = 3.45$  Hz) LC/MS 96.3%,  $[M]^- = 549.3$   $t_R = 8.28$  min. HRMS (ESI) (M+1): 551.1813 calcd for  $C_{28}H_{22}F_4N_6O_2$  (M+1): 551.1740. 54.3% yield.

**10.1.5. 5-(3-Fluoro-4-methylphenyl)-N-(4-methyl-3-(3-methyl-4-oxo-3,4-dihydroquinazolin-6-ylamino)phenyl)-2-(trifluoromethyl)-1H-imidazole-4-carboxamide (KIN038)**

$^1H$  NMR (300 MHz, acetone- $d_6$ ):  $\delta$  13.1 (br s, 1H, imid NH), 9.61 (br s, 1H, NH), 8.06 (s, 1H, Ar), 7.93 (d, 1H,  $J = 2.0$  Hz), 7.75 (dd, 1H,  $J = 1.6$  Hz,  $J = 11.3$  Hz), 7.59 (m, 2H), 7.42–7.56 (m, 2H), 7.22–7.35 (m, 3H), 3.52 (s, 3H), 2.24 (d, 3H,  $J = 10.4$  Hz), 2.10 (s, 3H).  $^{13}C$  NMR (75 MHz, acetone- $d_6$ ):  $\delta$  161.87 (d,  $J = 246.4$  Hz), 160.11, 160.19, 145.06, 144.93, 142.15, 141.13, 138.11, 136.50, 134.32 (q,  $J = 41.6$  Hz), 133.39 (d,  $J = 5.2$  Hz), 131.95, 131.48, 129.79 (d,  $J = 8.5$  Hz), 128.77, 126.30, 124.74, 124.504 (d,  $J = 17.8$  Hz), 123.95, 123.38, 119.24 (q,  $J = 269.0$ ), 115.39, 114.86 (d,  $J = 22.9$ ), 113.10, 109.40, 33.36, 17.243, 14.04 (d,  $J = 3.7$  Hz). LC/MS 96.3%,  $[M]^- = 549.3$   $t_R = 8.36$  min. HRMS (ESI) (M+1): 550.1816 calcd for  $C_{28}H_{22}F_4N_6O_2$  (M+1): 550.1740. 53.6% yield.

**10.1.6. N-(4-Methyl-3-(3-methyl-4-oxo-3,4-dihydroquinazolin-6-ylamino)phenyl)-2-(trifluoromethyl)-5-(3,4,5-trimethoxyphenyl)-1H-imidazole-4-carboxamide (KIN039)**

$^1H$  NMR (300 MHz, acetone- $d_6$ ):  $\delta$  13.0 (br s, 1H, imid NH), 9.58 (br s, 1H, NH), 8.07 (s, 1H, Ar), 8.02 (d,  $J = 1.6$  Hz), 7.66 (d,  $J = 2.1$  Hz), 7.5–7.6 (m, 2H), 7.44 (dd, 1H,  $J = 1.9$  Hz,  $J = 6.1$  Hz), 7.34 (s, 2H), 7.31 (s, 1H), 7.23 (d, 1H,  $J = 6.3$  Hz), 3.78 (s, 6H), 3.51 (s, 3H), 2.26 (s, 3H).  $^{13}C$  NMR (75 MHz, acetone- $d_6$ ):  $\delta$  161.14, 160.26, 153.36, 145.12, 144.71, 142.32, 141.25, 139.50, 138.106, 137.50, 133.91 (q,  $J = 38.9$  Hz), 131.46, 128.77, 125.78, 124.21, 123.76, 123.37, 119.05 (q,  $J = 268.8$  Hz), 115.07, 112.49, 109.81, 107.66, 107.44, 60.09, 55.99 (2C), 33.34, 17.22. LC/MS 98.23%,  $[M]^- = 607.4$   $t_R = 7.816$  min. HRMS (ESI) (M+1): 609.2068 calcd for  $C_{30}H_{27}F_3N_6O_5$  (M+1): 609.1995. 40.8% yield.

**10.1.7. N-(4-Methyl-3-(3-methyl-4-oxo-3,4-dihydroquinazolin-6-ylamino)phenyl)-2-(trifluoromethyl)-5-(3-(trifluoromethyl)-phenyl)-1H-imidazole-4-carboxamide (KIN040)**

$^1H$  NMR (300 MHz, acetone- $d_6$ ):  $\delta$  13.21 (br s, 1H, imid NH), 9.62 (br s, 1H, NH), 8.21–8.25 (m, 2H), 8.06 (s, 1H), 7.90 (s, 1H), 7.59 (d, 1H,  $J = 2.5$  Hz), 7.44–7.54 (m, 3H), 7.32 (s, 1H), 7.23 (d, 1H,  $J = 7.7$  Hz), 3.514 (s, 3H), 2.185 (s, 3H).  $^{13}C$  NMR (75 MHz, acetone- $d_6$ ):  $\delta$  161.12, 160.02, 148.88, 145.05, 144.86, 142.24, 141.16, 137.98, 135.92, 134.44 (q,  $J = 40.5$  Hz), 134.40, 134.02, 132.51, 131.50, 130.10 (q,  $J = 31.9$  Hz), 129.70, 128.79, 126.62 (q,  $J = 3.9$  Hz), 126.08 (q,  $J = 3.75$  Hz), 125.50, 124.91 (q,  $J = 228.5$  Hz), 123.90, 118.95 (q,  $J = 261.8$  Hz), 115.47, 113.14, 109.48, 33.35, 17.25. LC/MS 95.54%,  $[M]^- = 585.3$   $t_R = 6.87$  min. HRMS (ESI) (M+1): 587.1625 calcd for  $C_{28}H_{20}F_6N_6O_2$  (M+1) = 587.1552. 46.4% yield.

**10.1.8. N-(4-Methyl-3-(3-methyl-4-oxo-3,4-dihydroquinazolin-6-ylamino)phenyl)-2-(trifluoromethyl)-5-(2-(trifluoromethyl)-phenyl)-1H-imidazole-4-carboxamide (KIN041)**

$^1H$  NMR (300 MHz, acetone- $d_6$ ):  $\delta$  13.0 (br s, 1H, imid NH), 9.49 (br s, 1H, NH), 8.10 (dd, 1H,  $J = 2.2$  Hz,  $J = 5.2$  Hz), 7.82–7.86 (m, 2H), 7.65–7.75 (m, 3H), 7.49–7.54 (m, 3H), 7.42 (dd, 1H,  $J = 2.7$  Hz,  $J = 8.8$  Hz), 7.40 (s, 1H), 7.20 (d, 1H,  $J = 8.8$  Hz), 3.52 (s, 3H), 2.29 (s, 3H).  $^{13}C$  NMR (75 MHz, acetone- $d_6$ ):  $\delta$  161.08, 159.36, 148.89, 145.01, 142.15, 141.10, 138.05, 134.44 (q,  $J = 40.5$  Hz), 134.41, 133.45, 132.23, 131.45, 130.26, 129.94, 129.55 (q,  $J = 30.0$  Hz), 128.76, 126.50, 126.29 (q, 5.18 Hz), 125.50, 124.02 (q,  $J = 271.3$  Hz), 123.76, 122.55, 119.04 (q,  $J = 267.2$  Hz), 115.40, 113.28, 109.39 LC/MS 98.10%,  $[M]^- = 585.3$   $t_R = 6.56$  min. HRMS (ESI) (M+1): 587.1625 calcd for  $C_{28}H_{20}F_6N_6O_2$  (M+1) = 587.1552. 56.7% yield.

**10.1.9. 5-(3-Chloro-4-fluorophenyl)-N-(4-methyl-3-(3-methyl-4-oxo-3,4-dihydroquinazolin-6-ylamino)phenyl)-2-(trifluoromethyl)-1H-imidazole-4-carboxamide (KIN036)**

$^1H$  NMR (300 MHz, acetone- $d_6$ ):  $\delta$  13.0 (br s, 1H, imid NH), 9.59 (br s, 1H, NH), 8.10 (dd, 1H,  $J = 2.2$  Hz,  $J = 5.2$  Hz), 7.95 (s, 1H), 7.8–7.9 (m, 2H), 7.61 (d, 1H,  $J = 2.4$  Hz), 7.4–7.58 (m, 3H) 7.37 (t, 1H,  $J = 8.9$  Hz), 7.30 (s, 1H), 7.24 (d, 1H,  $J = 8.3$  Hz), 3.51 (s, 3H), 2.26 (s, 3H).  $^{13}C$  NMR (75 MHz, acetone- $d_6$ ):  $\delta$  161.17, 160.02, 158.47 (d,  $J = 248.32$ ), 145.03, 144.85, 142.27, 141.14, 137.98, 135.23, 134.76 (q,  $J = 41.3$  Hz), 132.32, 132.17, 131.48, 130.79 (d,  $J = 7.65$  Hz), 128.84, 126.71, 126.32, 124.02, 123.35, 120.13 (d,  $J = 17.65$  Hz), 118.99 (q,  $J = 267.3$  Hz), 116.62 (d,  $J = 21.3$  Hz), 115.37, 112.99 (d, 3.3 Hz), 109.37, 33.35, 17.25. LC/MS 96.86%,  $[M]^- = 569.3$   $t_R = 8.012$  min. HRMS (ESI) (M+1): 571.1267 calcd for  $C_{27}H_{19}ClF_4N_6O_2$  (M+1) = 571.1194.

**10.1.10. N-(4-Methyl-3-(3-methyl-4-oxo-3,4-dihydroquinazolin-6-ylamino)phenyl)-2,5-diphenyl-1H-imidazole-4-carboxamide (KIN043)**

$^1H$  NMR (300 MHz, acetone- $d_6$ ):  $\delta$  13.0 (br s, 1H, imid NH), 9.89 (br s, 1H, NH), 8.19 (d, 2H,  $J = 7.2$  Hz), 8.13 (s, 1H), 8.02 (s, 1H), 7.8–7.9 (m, 3H), 7.32–7.54 (m, 10H), 7.21 (d, 1H,  $J = 8.4$  Hz), 3.45 (s, 3H), 2.16 (s, 3H).  $^{13}C$  NMR (75 MHz, acetone- $d_6$ ):  $\delta$  161.87, 161.34, 149.81, 147.72, 145.67, 145.55, 141.59, 140.00, 138.58, 136.12, 135.14, 132.05, 131.81, 130.33, 130.23, 129.83, 129.54, 129.07, 128.69, 126.75, 125.67, 123.83, 123.28, 116.09, 114.255, 108.32, 34.26, 18.30. HRMS (ESI) (M+1): 527.2190 calcd for  $C_{32}H_{26}N_6O_2$  (M+1) = 527.2117. 73.6% yield.

**10.1.11. 2-tert-Butyl-N-(4-methyl-3-(3-methyl-4-oxo-3,4-dihydroquinazolin-6-ylamino)phenyl)-5-p-tolyl-1H-imidazole-4-carboxamide (KIN042)**

$^1H$  NMR (300 MHz, acetone- $d_6$ ):  $\delta$  11.30 (br s, 1H, imid NH), 9.62 (s, 1H, NH), 8.04 (s, 1H), 7.90 (d, 1H,  $J = 1.9$  Hz), 7.75 (d, 2H,

$J = 8.2$  Hz), 7.52–7.58 (m, 2H), 7.40–7.47 (m, 2H), 7.32 (s, 1H), 7.17–7.24 (m, 3H), 3.52 (s, 3H), 2.33 (s, 3H), 2.24 (s, 3H), 1.43 (s, 9H). 161.45, 161.09, 155.03, 145.22, 144.95, 142.12, 141.05, 138.65, 138.18, 134.80, 131.50, 129.49 (2C), 129.38, 128.83, 128.68 (2C), 127.46, 125.50, 123.59, 123.49, 115.07, 113.19, 109.14, 33.33, 33.06, 28.60 (3C), 20.78, 17.25. LC/MS 98.57%,  $[M]^- = 569.3$   $t_R = 8.133$  min. HRMS (ESI) (M+1): 521.2660 calcd for  $C_{31}H_{32}N_6O_2$  (M+1) = 521.2587. 57.4% yield.

#### 10.1.12. 4-(3,4-Difluorophenyl)-N-(4-methyl-3-(3-methyl-4-oxo-3,4-dihydroquinazolin-6-ylamino)phenyl)-2-(trifluoromethyl)-1H-imidazole-5-carboxamide (KIN057)

$^1H$  NMR (300 MHz, acetone- $d_6$ ):  $\delta$  13.25 (br s, 1H, imid NH), 9.60 (br s, 1H, NH), 8.06 (s, 1H), 7.98–8.06 (m, 1H), 7.91 (s, 1H), 7.7–7.8 (m, 1H), 7.61 (d, 1H,  $J = 2.4$  Hz), 7.33–7.63 (m, 4H), 7.30 (s, 1H), 7.24 (d, 1H,  $J = 8.2$  Hz), 3.53 (s, 3H), 2.26 (s, 3H).  $^{13}C$  NMR (75 MHz, acetone- $d_6$ ):  $\delta$  161.27, 160.02, 152.53 (d,  $J = 12.5$  Hz), 151.42 (d,  $J = 13.0$  Hz), 144.20 (d,  $J = 12.5$  Hz), 148.17 (d,  $J = 12.8$  Hz), 145.03, 144.90, 142.28, 141.18, 137.95, 134.92, 134.76 (q,  $J = 40.9$  Hz), 131.48, 128.81, 126.89 (m), 126.50, 123.93, 123.41, 119.51 (d,  $J = 18.9$  Hz), 118.97 (q,  $J = 264.7$  Hz), 117.34 (d,  $J = 21.6$ ), 115.48, 113.21, 109.47, 33.30, 17.21. LC/MS 96.84%,  $[M]^- = 553.2$   $t_R = 7.6816$  min. HRMS (ESI) (M+1): 555.1562 calcd for  $C_{27}H_{19}ClF_4N_6O_2$  (M+1) = 555.1490.

## 11. Computational methods

### 11.1. FLEXX Docking

Molecular modeling calculations were performed using the SYBYL 7.2 package (Tripos, St. Louis). All docking calculations were performed using FLEXX as implemented in SYBYL 7.2. Docking calculations were carried out using standard default parameters for the FLEXX program. The FLEXX program generates total a 30 of docking orientations for each ligand. FLEXX scores and orientations were used for the analysis. The best docking orientations from FLEXX were refined using the FLEXIDOCK program.

### 11.2. FLEXIDOCK

Docking of the molecules was performed using the FLEXIDOCK program available within the SYBYL 7.2 package. FLEXIDOCK utilizes both flexible rotatable bonds of the ligand and flexible protein to explore the biologically active conformation within the active site of the protein. Docking studies were performed for 10,000 generations, and only the energetically favorable conformations are analyzed. A total of 20 orientations were generated for each ligand and these were analyzed on the basis of the FLEXIDOCK score and their interaction within the active site.

### 11.3. Molecular overlap

Three-dimensional crystal structures of Gleevec® bound to C-Abl (2HYI), Sorafenib bound to B-Raf (1UWH), and BIRB-796 bound to p38 $\alpha$  (1KV2) were downloaded from Protein Data Bank. Water molecules were removed from each crystal structure, and monomers of 1KV2 and 1UWH were aligned with 2HYI using PVMOL v1.1 from Delano Scientific.

## 12. Biological evaluation

### 12.1. General

All assays utilized assay dilution buffer and Mg/ATP cocktail purchased from Millipore. The assay dilution buffer contained

20 mM MOPS, pH 7.2, 25 mM  $\beta$ -glycerophosphate, 5 mM EGTA, 1 mM  $Na_3VO_4$ , and 1 mM dithiothreitol (Millipore Catalog #20-108). The Mg/ATP cocktail contained 75 mM  $MgCl_2$ , and 0.5 mM cold ATP in Assay Dilution Buffer (Millipore Catalog #20-113). [ $\gamma$ - $^{32}P$ ] Adenosine-5'-triphosphate (10  $\mu Ci/\mu L$ ) was purchased from Perkin-Elmer and used at 0.8  $\mu Ci/rxn$ . Stock 10 mM drug solutions were made in DMSO and from that were diluted in a half-log manner in ddH $_2O$ . A minimum of three independent experiments were performed in the determination of IC $_{50}$  values.

### 12.2. B-Raf V600E enzymatic assay

7.5 ng Mouse Full-Length GST-tagged B-Raf V600E (Invitrogen, PV3849) was preincubated at room temperature for 1 h with 1  $\mu L$  drug and 4  $\mu L$  assay dilution buffer. The kinase assay was initiated when 5  $\mu L$  of a solution containing 200 ng recombinant human full length, N-terminal His-tagged MEK1 (Invitrogen, PV3093), 200  $\mu M$  ATP (0.8  $\mu Ci$  hot ATP), and 30 mM  $MgCl_2$  in assay dilution buffer was added. The kinase reaction was allowed to continue at room temperature for 25 min and was then quenched with 5  $\mu L$  5 $\times$  protein denaturing buffer (LDS) solution. Protein was further denatured by heating for 5 min at 70  $^\circ C$ . 10  $\mu L$  of each reaction was loaded into a 15-well, 4–12% precast NuPage gel (Invitrogen) and run at 200 V, and upon completion, the front, which contained excess hot ATP, was cut from the gel and discarded. The gel was then dried and developed onto a phosphor screen, which was scanned on a Storm 820 scanner and quantitated from optical densitometry using Image Quant v5.0. A reaction that contained no active enzyme was used as a negative control, and a reaction without inhibitor was used as the positive control. Final compound concentrations were 100  $\mu M$ , 31.6  $\mu M$ , 10  $\mu M$ , 3.16  $\mu M$ , 1  $\mu M$ , 316 nM, 100 nM, 31.6 nM, 10 nM, 3.16 nM, 1 nM, 316 pM, and 100 pM.

### 12.3. p38 $\alpha$ Enzymatic assay

The p38 $\alpha$  biological assay used the same protocol as B-Raf except it utilized recombinant human full length N-terminal GST-tagged p38 $\alpha$  (Invitrogen, PV3304) and recombinant human full length, N-terminal His-tagged MAPKAP-K2 (SPV3316).

## Acknowledgments

This research was supported by a grant from the National Foundation for Cancer Research. We are grateful to David Bishop for preparing, proofreading, and editing the final version of the manuscript and figures.

## References and notes

- Garnett, M. J.; Marais, R. *Cancer Cell* **2004**, 6, 313.
- Ishimura, N.; Yamasawa, K.; Karim Rumi, M. A.; Kadowaki, Y. *Cancer Lett.* **2003**, 199, 169.
- Li, N.; Batt, D.; Warmuth, M. *Curr. Opin. Invest. Drugs* **2007**, 8, 452.
- Tuveson, D. A.; Weber, B. L.; Herlyn, M. *Cancer Cell* **2003**, 4, 95.
- Kumar, R.; Angelini, S.; Czene, K.; Sauroja, I.; Hahka-Kemppinen, M. *Clin. Cancer Res.* **2003**, 9, 3362.
- Fukushima, T.; Suzuki, S.; Mashiko, M.; Ohtake, T.; Endo, Y.; Takebayashi, Y.; Sekikawa, K.; Hagiwara, K.; Takenoshita, S. *Oncogene* **2003**, 22, 6455.
- Davies, H.; Bignell, G. R.; Cox, C.; Stephens, P.; Edkins, S.; Clegg, S.; Teague, J.; Floyd, Y.; Gray, K.; Hall, S.; Hawes, R.; Hughes, J.; Kosmidou, V.; Menzies, A.; Mould, C.; Parker, A.; Stevens, C.; Watt, S.; Hooper, S.; Wilson, R.; Jayatilake, H.; Gusterson, B. A.; Cooper, C.; Shipley, J.; Hargrave, D.; Pritchard-Jones, K.; Maitland, N.; Chenevix-Trench, G.; Riggins, G. J.; Bigner, D. D.; Palmieri, G.; Cossu, A.; Flanagan, A.; Nicholson, A.; Ho, J. W.; Leung, S. Y.; Yuen, S. T.; Weber, B. L.; Seigler, H. F.; Darrow, T. L.; Paterson, H.; Marais, R.; Marshall, C. J.; Wooster, R.; Stratton, M. R.; Futreal, P. A. *Nature* **2002**, 417, 949.
- Zhang, B. H.; Guan, K. L. *EMBO J.* **2000**, 19, 5429.
- Wan, P. T.; Garnett, M. J.; Roe, S. M.; Lee, S.; Niculescu-Duvaz, D.; Good, V. M.; Jones, C. M.; Marshall, C. J.; Springer, C. J.; Barford, D.; Marais, R. *Cell* **2004**, 116, 855.

10. McCubrey, J. A.; Steelman, L. S.; Hoyle, P. E.; Blalock, W. L.; Weinstein-Oppenheimer, C.; Franklin, R. A.; Cherwinski, H.; Bosch, E.; McMahon, M. *Leukemia* **1998**, *12*, 1903.
11. Ng, R.; Chen, E. X. *Curr. Clin. Pharmacol.* **2006**, *1*, 223.
12. Eisen, T.; Ahmad, T.; Flaherty, K. T.; Gore, M.; Kaye, S.; Marais, R.; Gibbens, I.; Hackett, S.; James, M.; Schuchter, L. M.; Nathanson, K. L.; Xia, C.; Simantov, R.; Schwartz, B.; Poulin-Costello, M.; O'Dwyer, P. J.; Ratain, M. J. *Br. J. Cancer* **2006**, *95*, 581.
13. Sharma, A.; Tran, M. A.; Liang, S.; Sharma, A. K.; Amin, S.; Smith, C. D.; Dong, C.; Robertson, G. P. *Cancer Res.* **2006**, *66*, 8200.
14. Adnane, L.; Trail, P. A.; Taylor, I.; Wilhelm, S. M. *Methods Enzymol.* **2006**, *407*, 597.
15. Wilhelm, S. M.; Carter, C.; Tang, L.; Wilkie, D.; McNabola, A.; Rong, H.; Chen, C.; Zhang, X.; Vincent, P.; McHugh, M.; Cao, Y.; Shujath, J.; Gawlak, S.; Eveleigh, D.; Rowley, B.; Liu, L.; Adnane, L.; Lynch, M.; Auclair, D.; Taylor, I.; Gedrich, R.; Voznesensky, A.; Riedl, B.; Post, L. E.; Bollag, G.; Trail, P. A. *Cancer Res.* **2004**, *64*, 7099.
16. Sulzbacher, I.; Birner, P.; Traxler, M.; Marberger, M.; Haitel, A. *Am. J. Clin. Pathol.* **2003**, *120*, 107.
17. Tsuchiya, N.; Sato, K.; Akao, T.; Kakinuma, H.; Sasaki, R.; Shimoda, N.; Satoh, S.; Habuchi, T.; Ogawa, O.; Kato, T. *Tohoku J. Exp. Med.* **2001**, *195*, 101.
18. Hagiwara, K.; Takada, M.; Maruyama, M.; Matsuda, M.; Hatano, R.; Mitsui, J.; Sano, S. Preparation of imidazole derivatives as pest control drugs. *PCT Int. Appl.*, 1995; p 66. CODEN: PIXXD2 WO9504724.
19. Gotthardt, H.; Huisgen, R.; Bayer, H. O. *J. Am. Chem. Soc.* **1970**, *92*, 4340.
20. Peddibhotla, S.; Tepe, J. J. *J. Am. Chem. Soc.* **2004**, *126*, 12776.
21. Padwa, A.; Akiba, M.; Cohen, L. A.; MacDonald, J. G. *J. Org. Chem.* **1983**, *48*, 695.
22. *Synthetic Applications of 1,3-Dipolar Cycloaddition Chemistry Toward Heterocycles and Natural Products*; Padwa, A., Pearson, W. H., Eds.; Wiley, 2002.
23. Aquila, B.; Dakin, L.; Ezhuthachan, J.; Lee, S.; Lyne, P.; Pontz, T.; Zheng, X.-L. Preparation of Quinazolinone Derivatives as B-Raf Inhibitors. *PCT Int. Appl.*, 2006; p 112.
24. Pargellis, C.; Tong, L.; Churchill, L.; Cirillo, P. F.; Gilmore, T.; Graham, A. G.; Grob, P. M.; Hickey, E. R.; Moss, N.; Pav, S.; Regan, J. *Nat. Struct. Biol.* **2002**, *9*, 268.
25. Karin, M. *Proc. Am. Thorac. Soc.* **2005**, *2*, 386.
26. Genovese, M. C. *Arthritis Rheum.* **2009**, *60*, 317.
27. LoGrasso, P. V.; Frantz, B.; Rolando, A. M.; O'Keefe, S. J.; Hermes, J. D.; O'Neill, E. A. *Biochemistry* **1997**, *36*, 10422.
28. Tsai, J.; Lee, J. T.; Wang, W.; Zhang, J.; Cho, H.; Mamo, S.; Bremer, R.; Gillette, S.; Kong, J.; Haass, N. K.; Sproesser, K.; Li, L.; Smalley, K. S.; Fong, D.; Zhu, Y. L.; Marimuthu, A.; Nguyen, H.; Lam, B.; Liu, J.; Cheung, I.; Rice, J.; Suzuki, Y.; Luu, C.; Settachatgul, C.; Shellooe, R.; Cantwell, J.; Kim, S. H.; Schlessinger, J.; Zhang, K. Y.; West, B. L.; Powell, B.; Habets, G.; Zhang, C.; Ibrahim, P. N.; Hirth, P.; Artis, D. R.; Herlyn, M.; Bollag, G. *Proc. Natl. Acad. Sci. U.S.A.* **2008**, *105*, 3041.
29. Regan, J.; Breitfelder, S.; Cirillo, P.; Gilmore, T.; Graham, A.; Hickey, E.; Klaus, B.; Madwed, J.; Moriak, M.; Moss, N.; Pargellis, C.; Pav, S.; Proto, A.; Swinamer, A.; Tong, L.; Torcellini, C. *J. Med. Chem.* **2002**, *45*, 2994.
30. Fabian, M. A.; Biggs, W. H., 3rd; Treiber, D. K.; Atteridge, C. E.; Azimioara, M. D.; Benedetti, M. G.; Carter, T. A.; Ciceri, P.; Edeen, P. T.; Floyd, M.; Ford, J. M.; Galvin, M.; Gerlach, J. L.; Grotzfeld, R. M.; Herrgard, S.; Insko, D. E.; Insko, M. A.; Lai, A. G.; Lélias, J. M.; Mehta, S. A.; Milanov, Z. V.; Velasco, A. M.; Wodicka, L. M.; Patel, H. K.; Zarrinkar, P. P.; Lockhart, D. J. *Nat. Biotechnol.* **2005**, *23*, 329.